AFFDL-TR-78-141

LEVEL

AIRFRAME AERODYNAMIC NOISE — TOTAL RADIATED ACOUSTIC POWER APPROACH

STRUCTURAL INTEGRITY BRANCH
STRUCTURAL MECHANICS DIVISION

NOVEMBER 1978

TECHNICAL REPORT AFFDL-TR-78-141
Final Report for Period January 1976 -- January 1978

AIR FORCE FLIGHT DYNAMICS LABORATORY
AIR FORCE WRIGHT AERONAUTICAL LABORATORIES
AIR FORCE SYSTEMS COMMAND
WRIGHT-PATTERSON AIR FORCE BASE, OHIO 45433

NOTICE

When Government drawings, specifications, or other data are used for any purpose other than in connection with a definitely related Government procurement operation, the United States Government thereby incurs no responsibility nor any obligation whatsoever; and the fact that the government may have formulated, furnished, or in any way supplied the said drawings, specifications, or other data, is not to be regarded by implication or otherwise as in any manner licensing the holder or any other person or corporation, or conveying any rights or permission to manufacture, use, or sell any patented invention that may in any way be related thereto.

This report has been reviewed by the Information Office (OI) and is releasable to the National Technical Information Service (NTIS). At NTIS, it will be available to the general public, including foreign nations.

This technical report has been reviewed and is approved for publication.

Leonard L Shaw
LEONARD L. SHAW
Project Engineer

Philip A. Parmley
PHILLIP PARMLEY, Atg. Chief
Structural Integrity Br.
Structural Mechanics Div.

FOR THE COMMANDER

Ralph L. Kuster Jr.
RALPH L. KUSTER, Jr., Colonel, USAF
Chief, Structural Mechanics Division

Copies of this report should not be returned unless return is required by security considerations, contractual obligations, or notice on a specific document.

AIR FORCE/56780/19 December 1978 — 275

Unclassified

SECURITY CLASSIFICATION OF THIS PAGE (When Data Entered)

REPORT DOCUMENTATION PAGE

READ INSTRUCTIONS BEFORE COMPLETING FORM

1. REPORT NUMBER	2. GOVT ACCESSION NO.	3. RECIPIENT'S CATALOG NUMBER
AFFDL-TR-78-141		

4. TITLE (and Subtitle)
Airframe Aerodynamic Noise - Total Radiated Acoustic Power Approach.

5. TYPE OF REPORT & PERIOD COVERED
Final Jan 76 - Jan 78

6. PERFORMING ORG. REPORT NUMBER

7. AUTHOR(s)
L.L. Shaw
Leonard L. Shaw

8. CONTRACT OR GRANT NUMBER(s)

9. PERFORMING ORGANIZATION NAME AND ADDRESS
Acousitcs & Sonic Fatigue Group
Structural Integrity Branch
Structural Mechanics Div/AFWAL/AFFDL/FBE/WPAFB,OH

10. PROGRAM ELEMENT, PROJECT, TASK AREA & WORK UNIT NUMBERS
24011108

11. CONTROLLING OFFICE NAME AND ADDRESS
Acoustics & Sonic Fatigue Group
Structural Integrity Branch
Structural Mechanics Div/AFWAL/AFFDL/FBE/WPAFB,OH

12. REPORT DATE
November 1978

13. NUMBER OF PAGES
79

14. MONITORING AGENCY NAME & ADDRESS(if different from Controlling Office)

15. SECURITY CLASS. (of this report)
Unclassified

15a. DECLASSIFICATION/DOWNGRADING SCHEDULE

16. DISTRIBUTION STATEMENT (of this Report)
Approved for Public Release, Distribution Unlimited

17. DISTRIBUTION STATEMENT (of the abstract entered in Block 20, if different from Report)

18. SUPPLEMENTARY NOTES

19. KEY WORDS (Continue on reverse side if necessary and identify by block number)
Aerodynamic Noise, Acoustics, Accustic Power, Noise Prediction, Sailplane.

20. ABSTRACT (Continue on reverse side if necessary and identify by block number)
During flight the noise radiated by aircraft is emanating from two distinct types of sources. One source is the propulsion system and the other is the non-propulsion system noise, or airframe noise, associated with movement of the aircraft through the atmosphere. The purpose of this effort was to study the airframe noise using a total radiated acoustic power approach. Methodology was developed to accurately calculate the total acoustic power by using measurements from an array of microphones during aircraft flyover. This methodology was applied to Schweizer 2-32 glider flyovers and it was found that for an aerodynamic

DD FORM 1 JAN 73 1473 EDITION OF 1 NOV 65 IS OBSOLETE

Unclassified

SECURITY CLASSIFICATION OF THIS PAGE (When Data Entered)

(Block #20,Cont'd)
configuration (no flaps, wheels, wheel wells, etc.) the total acoustic power can be obtained from one flyover measurement by assuming the directivity is nearly equal in all directions. This assumption was shown to be valid for the glider and is assumed valid for any aircraft in an aerodynamic configuration. The detailed methodology developed is still useful since most commercial aircraft land in a non-aerodynamic configuration and thus their directivity is not equal in all directions. The results from the glider tests were compared to data in the literature and found to agree well. Variation of the total power with aircraft velocity followed a V to the sixth power law. The parameter which normalizes the overall acoustic power from different aircraft was found to be the wing area.

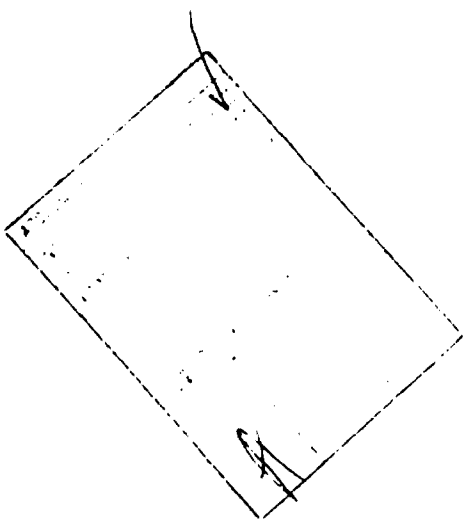

FOREWORD

This work was performed by the Structural Integrity Branch, Structural Mechanics Division, Air Force Flight Dynamics Laboratory, Wright-Patterson Air Force Base, Ohio. This effort was conducted under Work Unit 24010108, "Determination of the Total Radiated Acoustic Power from a Schweizer 2-32 Sailplane and Identification of the Noise Sources."

The work was performed by Mr. L.L. Shaw of the Structural Integrity Branch. This report presents and summarizes all of the work performed under this work unit.

The manuscript was released by the author in May 1978 as a technical report.

TABLE OF CONTENTS

LIST OF ILLUSTRATIONS

LIST OF ILLUSTRATIONS (CONT'D)

LIST OF TABLES

LIST OF SYMBOLS

A	Area - m^2
AR	Aspect Ratio - unitless
b	Wingspan - m
$\bar{c}$	Mean Airfoil Chord - m
C	Speed of Sound - m/s
C_D	Coefficient of Drag - unitless
DI	Directivity Index - dB
f	Frequency - Hertz
h	Altitude - m
I	Intensity - w/m^2
L_p	Sound Pressure Level - dB
L_w	Sound Power Level - dB
M	Mach Number - unitless
n	Integer - unitless
p	Acoustic Pressure - psi
R	Radial Distance - m
S	Wing Area - m^2
S_{TR}	Strouhal Number - unitless
t	Time; Wing Thickness s,m
v	Velocity - m/s
W	Acoustic Power - w
X	Distance Between Line of Flight and Microphones - m
α	Absorption Coefficient - dB/100m
c	Acoustic Impedence - Kg/m^2s
θ,ϕ	Angles - Degrees

SECTION I

INTRODUCTION AND BACKGROUND

The radiated noise associated with a flight vehicle is generated by two distinct types of sources: (1) the propulsion system, and (2) the non-propulsion system noise associated with movement of the vehicle through the atmosphere. The non-propulsion system noise is sometimes called airframe-aerodynamic noise or self-noise. In cases where the propulsion system noise is drastically reduced or totally eliminated, the airframe noise can become significant. For example, it is desired that light military reconnaissance-surveillance type aircraft operate as quietly as possible to avoid aural detection. The propulsion system noise from this type of aircraft can be reduced to the point where the airframe noise becomes the primary source. Thus, airframe noise can be considered as a noise floor or barrier that might prevent reaching the desired low noise levels.

Commercial transport aircraft also may have a problem with airframe noise. Noise reduction technology available today has the potential of reducing the propulsion system noise on commercial aircraft, during approach, to a level near or below the airframe noise. Any further reduction of the approach noise levels may require reducing the airframe noise levels. These further reductions may be required to meet the stringent FAR-36 noise requirements.

Only a limited amount of aerodynamic noise research has addressed the problem of airframe noise. The first large scale study of the airframe noise produced by actual aircraft was performed in 1970 by D.L. Smith et al (Reference 1). A series of noise measurements during flyovers of three

gliders were performed. An expression was derived which would predict the overall noise radiated from each of the sailplanes.

Since 1970 NASA, NAVY, and private industries have become active in airframe noise research and have published several reports on the subject. For example, in 1970 Healy (Reference 2), at the Lockheed-California Company, undertook a program to measure the noise of several gliding aircraft. In 1972 preliminary airframe noise measurements were made on a Boeing 747 aircraft and a Convair 990 (Reference 3). More recently, a joint Lockheed and NASA program (Reference 4) obtained airframe noise measurements on a C-5 Galaxy transport which verified that airframe noise could be a real "barrier" to overall noise reduction of large aircraft.

The main objective of this effort was to study airframe aerodynamic noise through the determination of the total radiated acoustic power from a Schweizer 2-32 sailplane and to relate aspects of the noise signature to various sources of the aircraft. The reason for choosing a Schweizer 2-32 sailplane is that flyover data from a previous test for several flights over an array of microphones were available to the author. A description of the test is given below:

The data used in this thesis were obtained during a flight program with a Schweizer 2-32 sailplane. The tests were conducted at Waynesville, Ohio, in November 1972. A picture of the sailplane is shown in Figure 1. Figure 2 shows the microphone array that was used to obtain the flyover data. Three microphones were in the flight path and six were in a line perpendicular to the flight path. Figure 3 gives the microphone spacings. The flight tests were conducted with the sailplane in level flight over the microphone array.

Table I shows the range of velocities and altitudes encompassed in the test and the velocity and altitude of the three flights selected for analysis. For each flyover noise measurement, the sailplane was towed to an altitude of approximately 1000 feet. After the tow plane had landed and shut down its engine, and ambient noise levels were determined to be sufficiently low, the sailplane approached the microphone array. The pilot attempted to maintain steady flight conditions from 100 feet ahead of the lead microphone to 100 feet beyond the last microphone.

A block diagram of the data acquisition system is shown in Figure 4. The signals from the nine microphone/cathode follower systems were amplified by high input impedance line drive amplifiers. The low impedance outputs from the amplifiers were transmitted through 1200 foot land lines to voltage amplifiers located in the AFFDL van. The outputs from the voltage amplifiers were recorded directly on a 14 channel Honeywell 7400 FM magnetic tape recorder. A microphone was used in the van to record on tape all pertinent data during the test. Wind velocity and direction measured at weather station were monitored in the van and recorded on magnetic tape. The motion picture camera generated an electronic signal each time the shutter was full open. This signal was transmitted to the van and recorded on magnetic tape for correlating the microphone data with sailplane location. Table II presents a list of the data acquisition instrumentation and calibration equipment used for the test. Further details about the test arrangement, data acquisition system, and test procedures are presented in Reference 1.

To meet the main objective of the effort, a methodology to determine the total radiated acoustic power was developed because one was not available

in the literature. The methodology considers the doppler effect in the data due to the moving source. Whenever the source, or the receiver, or both are in motion relative to the air, the pitch of the sound and its amplitude as heard by the receiver are, in general, not the same as when the source and receiver are at rest. Thus, this shift in frequency and amplitude must be taken into consideration. The methodology also takes into account spherical divergence and atmospheric absorption. The development of the methodology is presented in Section II.

Section III presents a discussion of the data reduction procedures used on the resulting data. The results of the overall acoustic power calculation are presented in Section IV. Comparisons of the results to other findings in the literature are also included. A summary of the conclusions and recommendations is given in Section V.

SECTION II

DEVELOPMENT OF METHODOLOGY TO DETERMINE TOTAL RADIATED POWER FROM FLYOVER MEASUREMENTS

The simplest method to evaluate a noise source to determine its efficiency as a noise generator is through the use of radiated acoustic power. The total overall radiated acoustic power is a single number which eliminates directivity effects; thus, given the acoustic power level of two different sources, one can make a judgment as to which one is the most or least efficient noise generator. Also, if the directivity of the source is known along with the power level, the sound pressure level at any direction or distance from the source can be determined. For these reasons, the radiated acoustic power and directivity approach was applied to the airframe noise problem.

The overall and one-third octave band radiated acoustic power levels, along with the associated directionality characteristics for the airframe noise of a Schweizer 2-32 glider, were determined. Before this could be done the necessary methodology had to be developed. This development process is described below:

The basic definition of acoustic power level is

$$L_W = 10 \log W/W_o \qquad (1)$$

where W_o is the standard power reference of 10^{-12} watts. The acoustic power is given by

$$W = IA \qquad (2)$$

where I is the acoustic intensity associated with an area A. To get the total power of a source, it is enclosed within an imaginary sphere with a total area of A. Since all of the radiated acoustic energy passes through the sphere, the total acoustic power is determined. If the source, in this case the glider, is directional the intensity will vary over the surface of the sphere necessitating dividing the sphere into numerous subareas and summing the power from each subarea to get the total power. The power is now written as

$$W_i = I_i A_i \tag{3}$$

$$W_{TOTAL} = \sum_{i=1}^{N} W_i \tag{4}$$

It is logical to assume that the smaller the subareas the more accurate the results will be. Of course, a point can be reached where decreasing the area further will result in only a negligible change in the results. For this effort, the number or size of subareas was set by the record sampling rate of the digital analyzer. The smallest sampling rate available was one-tenth of a second which was the one used.

Calculation of each subarea was performed by dividing the imaginary sphere into lunes in the direction of flight. This is illustrated in Figure 5 which also shows the spacing of the microphones in the array. The microphone spacing dictates the width of lunes. The width, in radians, of each lune can be determined as follows: Letting θ_i be the angle for the ith lune and h the altitude of the aircraft, the following expressions can be written:

$$\tan(\theta_1/2)=3.81/h \quad (5.a)$$

$$\tan(\theta_2+\theta_1/2)=15.24/h \quad (5.b)$$

$$\tan(\theta_3+\theta_2+\theta_1/2)=38.10/h \quad (5.c)$$

$$\tan(\theta_4+\theta_3+\theta_2+\theta_1/2)=83.82/h \quad (5.d)$$

By rearranging the expressions and noting symmetry, one can determine the final expressions that were used to calculate the lune widths for the glider flights. These are as follows:

$$\theta_1=2\tan^{-1}(3.81/h) \quad (6.a)$$

$$\theta_2=\theta_1=\tan^{-1}(15.24/h)-\tan^{-1}(3.81/h) \quad (6.b)$$

$$\theta_3=\theta_6=\tan^{-1}(38.10/h)-\tan^{-1}(15.24/h) \quad (6.c)$$

$$\theta_4=\theta_5=\tan^{-1}(83.82/h)-\tan^{-1}(38.10/h) \quad (6.d)$$

Application of these equations to other microphone arrays could easily be accomplished by entering the appropriate spacings. In order to fully define the subareas, each lune must be divided into smaller areas as shown in Figure 6. A typical lune is shown with a subarea indicated. The expression which was used to calculate these subareas is

$$A_{ij}=R^2\theta_i(\sin\phi_j-\sin\phi_{j-1}) \quad (7)$$

where R is the radius of the sphere, θ is the lune width in radians, and ϕ is the angle between a line from the aircraft to the microphones and a line perpendicular to the flight path. The sine functions must be expressed in terms of the flight parameters before they are useful. This is easily

accomplished with the aid of Figure 7. The imaginary sphere around the sailplane is shown for two instants in time. The horizontal distance is expressed in terms of flight velocity "v" and time. The vertical distance is simply the height above ground. Thus, the sine functions can be expressed as follows:

$$\sin \theta_j = vt_j/\sqrt{(vt_j)^2 + h^2} \tag{8.a}$$

$$\sin \phi_{j-1} = vt_j/\sqrt{(vt_{j-1})^2 + h^2} \tag{8.b}$$

The final expression for the subareas can now be expressed as

$$A_{ij} = R^2\theta_i(vt_j/\sqrt{(vt_j)^2 + h^2} - vt_{j-1}/\sqrt{(vt_{j-1})^2 + h^2}) \tag{9}$$

where θ_i is defined in equation 6. With the area term in equation 3 fully defined in terms of flight parameters, the next step is to define the intensity term.

The intensity term in equation 3 can be written as

$$I = p^2/\rho c \tag{10}$$

where P is the root mean square sound pressure and ρc is the characteristic impedance of the medium in which the sound is being propagated. From the basic definition of sound pressure level,

$$L_p = 10 \log[p^2/p^2_{ref}] \tag{11}$$

p^2 can be written as

$$p^2 = p^2_{ref} \log^{-1} (L_p/10) \tag{12}$$

The intensity now becomes

$$I = (p^2_{ref}/\rho c)\ \log^{-1}(L_p/10) \tag{13}$$

and thus the power for each incremental area is now

$$W_{ij} = (p^2_{ref}/\rho c)\ \log^{-1}(L_{pij}/10)R^2\theta_i\left(\frac{vt_j}{\sqrt{(vt_j)^2 + h^2}} - \frac{vt_{j-1}}{\sqrt{(vt_{j-1})^2 + h^2}}\right) \tag{14}$$

The only term that remains to be fully defined is L_{Pij}. This is the sound pressure level at the centers of the incremental areas on the surface of the imaginary sphere.

The levels measured near the ground during flyover must be corrected to account for several factors that alter the actual levels that exist on a sphere about a moving source. Among these, the most significant ones are spherical spreading (divergence losses), Doppler shift, and atmospheric absorption.

The magnitude of the correction which must be applied to the measured levels to correct for spherical spreading can be very large, especially for high flyover altitudes or large sideline measurement distances. This correction results from the spherical radiation of the airframe generated sound power. When a source radiates its acoustic energy spherically the total radiated acoustic power must be constant for any given radial distance from the source. That is

$$W_{r=1} = W_{r=2} = W_{r=2} \cdots \tag{15}$$

or

$$I_1A_1 = I_2A_2 = I_3A_3 \cdots \tag{16}$$

Since, $A_i = 4\pi r_j^2$, , Equation 16 becomes

$$I_1 4\pi r_1^2 = I_2 4\pi r_2^2 = I_3 4\pi r_3^2 \tag{17}$$

The intensity ratio is obviously

$$I_1/I_2 = r_2^2/r_1^2 \tag{18}$$

which is an inverse square relationship. As shown previously, the intensity can be written in terms of the sound pressure as

$$I_i = P_i^2/\rho c \tag{19}$$

In terms of intensity ratio this becomes

$$I_1/I_2 = P_1^2/P_2^2 = r_2^2/r_1^2 \tag{20}$$

which can be written as

$$r_2^2/r_1^2 = (P_1^2/P_{ref}^2)/(P_2^2/P_{ref}^2) \tag{21}$$

Taking ten times the logarithm of both sides yields

$$10\log(r_2^2/r_1^2) = 10\log[(P_1^2/P_{ref}^2)/(P_2^2/P_{ref}^2)] \tag{22.a}$$

$$10\log(r_2^2/r_1^2) = 10\log(P_1^2/P_{ref}^2) - 10\log(P_2^2/P_{ref}^2) \tag{22.b}$$

$$10_{\log}(r_2^2/r_1^2) = L_{p_1} - L_{p2} \tag{22.c}$$

Thus, the sound pressure level on the surface of the sphere, corrected only for spherical spreading, is given by

$$L_{p\ surface} = L_{p\ measured} + 20 \log (r_1/r_2) \tag{23}$$

where r_1 is the line of sight distance between the microphone in question and the center of the sphere and r_2 is the radius of the sphere. In terms of flight parameters r_1 can be expressed as

$$r_1 = \sqrt{X_i^2 + h^2 + (vt)^2} \tag{24}$$

where X_i is the horizontal distance between the flight path and the ith microphone, h is the altitude, V is the velocity, and t is the time before or after the overhead position. For the purpose of this report, the radius of the sphere was chosen to be 15.24 meters. Thus, the correction for spherical spreading is

$$20 \log(\sqrt{x_i^2 + h^2 + (vt)^2}/15.24) \tag{25}$$

This correction can be very large even for low altitude approaches and slow speeds. For example, with the following values:

$$X_i = 53.34m \qquad v = 41.76m/sec$$
$$h = 52.42m \qquad t = 5\ sec \tag{26}$$

the correction is 23 dB. The values are typical of a glider flyover.

Another source of variation in the measured levels that can be corrected for is Doppler effect. The Doppler effect exists whenever there is relative motion between a source and a receiver. In the case of an aircraft

flyover and a stationary ground receiver there will always be a Doppler effect. Both the frequency distribution of the radiated acoustic energy and the amplitude will be altered. The frequency correction will be discussed first and then a correction for the amplitude will be developed.

Figure 8 shows a moving source with radiated scund waves. It is readily evident that the wave length of the sound ahead of the source is less than that of a stationary source and the wave length behind the moving source is greater. The wave length expressed in terms of the speed of sound, velocity of the source, and the frequency becomes:

$$\lambda_a = \lambda_{ahead} = (c-v)/f \tag{27}$$

$$\lambda_b = \lambda_{behind} = (c+v)/f \tag{28}$$

The frequency of the sound measured is

$$f_m = f_{measured} = c/\lambda \tag{29}$$

Thus, ahead of the source this becomes

$$f_{ma} = C/\lambda_a \tag{30.a}$$

$$= c/(c-v)/f \tag{30.b}$$

$$= f/(1-V/C) \tag{30.c}$$

$$f_{ma} = f/(1-M) \tag{30.d}$$

and for behind the source

$$f_{mb} = f/(1+M) \tag{31}$$

In these expressions f is the actual radiated frequency of the source and f_m is the measured frequency. An important point to bring out is that the Mach number M must be the relative Mach number between the source and measurement point in question, not the horizontal Mach number. For an aircraft flyover with ground measurement positions off the flight path the relative Mach number will vary significantly from the horizontal Mach number. Figure 9 shows a partial layout of the microphones relative to the glider flying overhead. Theta is the angle between the horizon and a line between the center of the source and Microphone 1. Phi is the sideline angle locating the microphones to the side of the flight path. The relative Mach number at any location is determined by

$$M_{relative} = M\cos\theta\,\cos\phi \tag{32}$$

In terms of the flight parameters

$$\cos\theta = vt_j/\sqrt{h^2 + (vt_j)^2} \tag{33}$$

$$\cos\phi = \sqrt{h^2 + (vt_j)^2}\,/\,\sqrt{x_i^2 + h^2 + (vt_j)^2} \tag{34}$$

and thus

$$M_{relative} = Mvt_j/\sqrt{x_i^2 + h^2 + (vt_j)^2} \tag{35}$$

Finally, the measured frequencies ahead of and behind the source can be corrected for the Doppler shift using this expression for M_{rel} in equations 30 and 31.

The Doppler effect on the amplitude must also be considered. Normally this effect is small and is neglected. However, for the purpose of this study it will be investigated. Classically the instantaneous acoustic pressure ahead of a moving spherical source is given by (Reference 6)

$$P = \frac{q'(t-\frac{R}{c})}{4\pi R(1\pm M_{rel})^2} + \frac{q(\cos\theta - M_{rel})v}{4\pi R^2(1\pm M_{rel})^2} \tag{36}$$

where q is the total rate of mass flux and q' is the time rate of change of the mass flux. For a fairly large distance (R) between the source and receiver, which is usually the case for aircraft flyover measurements, the first term will dominate the two terms because R is raised to the -2nd power in the second term and only -1st power in the first term. Neglecting the second term, the instantaneous pressure can now be written

$$P = \frac{q'(t-\frac{R}{c})}{4\pi R(1\pm M_{rel})^2} \tag{37}$$

The sound pressure level is defined as

$$L_p = 10 \log (P/P_{ref})^2 \tag{38}$$

Inserting P from equation 37 gives

$$L_p = 10 \log\left[\frac{q'(t-R/C)}{P_{ref}\ 4\pi R\ (1 \pm M_{rel})^2}\right]^2 \tag{39}$$

Since only the change in the sound pressure level due to the relative motion of the source is of interest here, equation 30 can be reduced to

$$\Delta L_p = 10 \log \left[1/(1 \pm M_{rel})\right]^4 \qquad (40.a)$$

$$\Delta L_p = -40 \log (1 \pm M_{rel}) \qquad (40.b)$$

where the minus is for the case where the receiver is ahead of the source and the plus is for the receiver behind the source. For a typical glider flyover the values for ΔL_p ranged from zero at the overhead position to approximately 2 dB at a position five seconds before and after the overhead position.

The third source of deviation of the radiated acoustic energy is atmospheric absorption. As a sound wave travels through still homogeneous air it loses energy by two processes - classical and molecular absorption. Energy extracted from the wave through the effects of heat conduction and radiation, viscosity, and diffusion are referred to as the classical absorption losses. These losses are proportional to the frequency squared but are independent of the air. The molecular absorption losses are related to the molecular relaxation behavior of the oxygen molecules in the air. In simple terms, molecular absorption losses result from the difference in the relaxation time required for the translational and rotational energy of the molecules to reach equilibrium conditions. The corresponding two components of the specific heat will be out of phase in a periodic change of state. This results in a complex compressibility which causes losses. The molecular absorption losses

are a function of frequency, humidity, and temperature. Since the classical absorption levels are normally very much less than the molecular levels, they will not be considered in this study.

Reference 7 presents absorption values for sound in air as a function of humidity and temperature. These values were applied to the glider flights. Before the values could be determined the temperature and humidity of the air during the glider flyover had to be determined. The temperatures were recorded during the flights but the humidity, unfortunately, was not recorded. It was later obtained from meteorlogical data recorded at a nearby location and ranged from 63% to 70% during the course of the flights. An average value of 65% was used. The temperature ranged from 46°F to 56°F and an average temperature of 51°F was used. With these data the absorption values for several one-third octave and octave band center frequencies from 125 Hz to 5,000 Hz were determined from Reference 7 and are shown in Table III. It is evident that the atmosphere absorption at the lower frequencies is fairly low but at the higher frequencies becomes quite significant. In order to utilize these data in a program to calculate the acoustic power, a functional relationship between the frequency and absorption values must be derived. The relationship which was used is

$$\alpha = Af^{y} \quad \text{dB/100m} \tag{41}$$

where A and y were determined from the values in Table II giving the final form of the equation as

$$\alpha = 4.65 \times 10^{-5} f^{1.34} \quad \text{dB/100m} \tag{42}$$

Utilizing the above equations, the measured levels can be corrected for spherical spreading, Doppler shift, and atmospheric absorption. Other factors which vary with time and location are wind and temperature gradients, turbulent scattering, terrain attenuation, focusing, fog, and rain. Since these do vary with time and location they will not be addressed in this report. After the above three corrections are made, the sound pressure levels on the surface of the imaginary sphere about the glider are obtained and thus, all terms in Equation 14 have been defined. The acoustic power radiated through each incremental area can now be calculated. In order to apply Equation 14 to the glider flyovers, the indices of iteration must be defined. The ith index is controlled by the number of microphones in the array which, in this case, is 7. Therefore, i would range from 1 to 7. The jth index is controlled by the number of data samples taken during the flyover which is a function of the amount of usable data. Five seconds of data before and after the overhead position was utilized. For a sampling rate of 1/10 second this resulted in j varying from -50 to +50. With these values in Equation 14 the power radiated from that portion of the sphere results. If one assumes a dipole radiation pattern from the glider, the result from Equation 14 can be doubled to give the power over the upper and lower portions of the sphere. This still leaves a portion on each side of the sphere that is not accounted for yet. The percent of area on the sphere not accounted for is a function of aircraft velocity, altitude, and the microphone array. For a typical glider flyover this unaccounted for area was approximately 38% of the total area. If one assumes that the sound pressure level over this area can be approximated by the average level over the measured area, then an approximation for the total radiated

acoustic power is given by

$$W_T = 2.76 \sum_{i=1}^{i=7} \sum_{j=-50}^{j=50} (P_{ref}^2/\rho c) \log^{-1}(L_{pij}/10) R^2 \theta_i \left(\frac{vt_j}{\sqrt{(vt_j)^2 + h^2}} - \frac{vt_{j-1}}{\sqrt{(vt_{j-1})^2 + h^2}} \right) \quad (43.a)$$

and the power level is

$$L_w = 10 \log (W_T/10^{-72}) \quad (43.b)$$

The overall sound power level, L_w, gives one number with which comparisons can quite readily be made to noise criteria or other levels to determine which source is the most or least efficient noise generator. The effects of directivity are eliminated in this approach, thus, simplifying the comparison. The effects of spherical divergence, Doppler shift, and atmospheric absorption have been taken into consideration.

SECTION III

DATA REDUCTION AND ANALYSIS

a. Data Reduction Procedures

The data obtained during the flyovers were recorded on magnetic tapes. Data reduction of the measurements on the tapes was accomplished using the system shown in Figure 10. The magnetic tapes were played back in the laboratory on a Honeywell 7400 tape recorder/reproduce system. Overall time histories and one-third octave band analysis were performed using a General Radio 1926 multi-channel rms detector interfaced with a 2116 Hewlett-Packard digital computer. For each record the one-third octave band analysis was performed every 1/10 second using 1/10 second averaging time. All of the analyses were performed on a total of 10 seconds of data, 5 seconds before overhead position and 5 seconds after. Time before the overhead position was assigned negative values and time after overhead was assigned positive values. In some cases, especially at the lower frequencies, the data for time outside the interval of -2 and +2 seconds could not be used because the measured levels were below the ambient noise levels.

b. Time Histories

Time histories of the flyover noise levels were plotted for all three flyovers selected for analysis for each one-third octave band from 200 Hz to 5000 Hz and the overall level, and for microphones 1 and 4. This resulted in 96 time history plots.

Figures 11 and 12 present typical time histories for an altitude of 118 feet and velocity of 135 feet per second. Figure 11 shows the results from microphone 1 located directly under the flight path. The top curve is

the overall level and the other three are the 2,000, 2,500, and 4,000 Hz one-third octave bands. These data show typical trends observed in all the results. The 4,000 Hz curve is the lowest, which indicates the acoustic energy is at the lower frequencies. When the glider is approaching the array, the 2,500 Hz band is well above the 2,000 Hz band but after the glider has passed over the array the 2,000 Hz band is the higher. This could result if the directivity is different at each frequency. This will be discussed in detail in a later section. The figure reveals that the maximum level at certain frequencies does not occur at the overhead position because of the directivity. A significant fact to observe from the figure is the magnitude of the increase during the flyover. In general, the increase was 20 dB but it was as high as 30 dB, as can be seen in the Figure for the 2,500 Hz band. Figure 12 shows data from microphone 4 located 175 feet to the right of the flight path. One would readily assume the levels at this location would be much lower than directly under the flight path. The figure definitely shows this. The decrease is not the same for the entire flyover; the largest decrease occurs near zero time. Again, the 2,500 Hz band is higher than the 2,000 Hz ahead of the glider and these reverse behind the glider. It can be assumed that the directivity effects at these frequencies are essentially the same at a side angle as they are directly below the glider.

c. One-Third Octave Band Spectra

One-third octave band spectra were plotted for the overhead position. A mean spectrum obtained from three flyovers is presented in Figure 13 for a frequency range of 160 Hz to 3150 Hz. The peaks in the spectrum at 200 Hz, 1,250 Hz, and 2,500 Hz indicate that there are distinct sources generating

that energy. In Reference 8, vortex generated noise is shown to give strong peaks in the radiated far-field environment of isolated airfoils. An expression offered in the reference to predict the frequency of this source is

$$f = \frac{.011V^{3/2}}{(C\nu)^{1/2}} \tag{44}$$

where V is the free stream velocity, C is the wing chord, and ν is the kinematic viscosity. Using the following values for the Schweizer 2-32

$V = 41.15$ M/sec

$c = 0.91$ (mean chord)

$\nu = 1.46 \times 10^{-5}$ m^2/sec

Equation 44 predicts a frequency of 795 Hz, which does not agree very well with the observed frequencies. However, if a chord dimension less than the mean chord is used in the equation the result would be much closer to the measured value. For example, using a chord of 14 inches, equation 44 predicts the 1,250 Hz peak very closely. This dimension is close to the tip chord on the glider. In Reference 9 another equation is presented for determining the tone frequencies. It was derived on the basis of stability theory which shows that the acoustic field and the wake flow could interact in a self-excited feedback mechanism which produces the tones. The equation is

$$f = 11.8nV^{0.8} \tag{45}$$

where n is an integer. For the velocity above, equation 45 gives $f = 597n$, or $n = 2$, $f = 1194$ Hz. This frequency agrees very well with the peak in the one-third octave band centered at 1250 Hz. The tone near 2500 Hz is predicted

by equation 45 for n = 4 which gives f = 2389 Hz. The agreement is again fairly good.

Neither of the above equations predicts the peak at the lower frequency. The n = 1 value from equation 45, 597 Hz, is much too high to be associated with the low frequency; thus, it is concluded that this source is not related to the airfoil trailing edge source. This is what the authors of Reference 10 concluded about the low frequency source. In Reference 11 a low frequency source related to the wing profile drag was identified. For the DC-3 this frequency was 120 Hz. It is assumed the energy at the low frequency for the glider flyover is also related to the wing profile drag. An expression presented in Reference 11 to predict this frequency is

$$f = S_{TR} V_{TE} / C_D \bar{c} \tag{46}$$

where S_{TR} is a Strouhal number, V_{TE} is the velocity at the trailing edge of the airfoil, C_D is the drag coefficient of the airfoil, and $\bar{c}$ is the mean chord. A Strouhal number of 0.1 was recommended (Reference 11) along with a V_{TE}/V ratio of 0.974. Using a drag coefficient of .005 and a mean chord of 3 feet for the Schweizer 2-32, the recommended values results in a frequency of 876 Hz for a flight velocity of 135 fps. This is much too high since the frequency was near 200 Hz. However, since the drag coefficient is a function of angle of attack, the true drag coefficient is difficult to ascertain. If we assume a drag coefficient of 0.01, which is still realistic, the predicted frequency becomes 438 Hz, which is much closer to the observed frequency. Due to the difficulty in determining the appropriate drag coefficient, this method is considered to be too refined for first-estimate type solutions.

In order to estimate a spectrum shape, the location of the maximum broadband level is needed. The most widely used expression to predict the peak in the broadband spectrum is

$$f = 1.3V/t \tag{47}$$

where t is the wing thickness and V is the velocity. This expression does not predict the frequency of the narrow band energy at the low frequency, but it predicts the frequency at which the broadband spectrum is maximum. It has been shown (Reference 10) that this expression gives acceptable accuracy. The shape of the spectrum is best described by Healy's (Reference 10) curve fit shown in Figure 14. This spectrum does not indicate any narrowband peaks at either the high or low frequencies. Cargo/transport type aircraft do not exhibit strong narrowband peaks like the gliders do; however, they do display broadband energy at these frequencies. This can be seen in Figure 15 from flyover data (Reference 3) for a B-747 and CV-990. Both high and low frequency humps are present in each of the flyovers but they are broadband. These peaks vary significantly with velocity or aircraft size, thus the smooth spectrum in Figure 14 can be modified to approximate these two noise sources. This was done by superimposing a 5 dB "hump" at the two normalized frequencies; the results being shown in Figure 16. This spectrum shape is recommended to predict the energy distribution for a "clean" aircraft flyover.

d. Directivity

There is still some controversy over the directivity of airframe noise. The authors of Reference 9 recommend a flyover measurement program involving an array of microphones to help resolve this controversy. The classic approach

is to apply Curle's dipole model to determine the directivity of the airfoils. This has been shown (Reference 9) to be valid for small airfoils; that is, for high wavelength to airfoil chord ratios ($\gg 1$). However, for larger airfoils (ratio $\lesssim 1$) the measured data do not substantiate Curle's dipole model. Since most aircraft have airfoil chord dimensions equal to or greater than the wavelength of interest, current understanding of the directivity of this source warrants further investigation. Based on this need, the directivity of the noise radiated from the Schweizer 2-32 was determined. The flyover measurements consisted of an array of microphones perpendicular to the flight path which yielded sufficient data to enable directivity determination.

The first step in determining the directional characteristics of the airframe noise was to calculate the total radiated acoustic power. This was accomplished utilizing the results of Section II. The power results will be discussed in greater detail in the next section. Knowing the radiated power level a space average $\bar{L}_p$ is obtained from the expression

$$\bar{L}_p = PWL - 20 \log R - 11 \tag{48}$$

where R is the radial distance in meters from the source. The Directivity Index (DI) for each angle θ is defined as

$$DI_\theta = L_{p\theta} - \bar{L}_p \tag{49}$$

The angle θ is measured from the direction of flight; $\theta = 0°$ is the direction of flight and $\theta = 90°$ is the overhead position.

Directivity plots were generated for each of the three flights analyzed: 23, 24, and 25. One-third octave band as well as overall L_p directivity plots were obtained. There were some variations in the data from each flight; however, these differences were small (2-3 db) and are attributed to the fact that the glider was not directly over microphone one on each flight. In view of this, emphasis is placed on the results of flight 23 and these are the only data presented in this section.

Figure 17 through 23 show the directivity indices for several one-third octave bands and the overall level. Data from all seven microphones are presented for angles from less than 30° to greater than 150°. This is considered a very adequate range of investigation since any noise radiated less than 30° has such a large distance to propagate to reach an observer on the ground that most of the acoustic energy would be dissipated by the time it reaches the observer. Figure 17 presents the results for the 200 Hz band. There is significant variation between the results from each microphone at the low frequencies. In general, the levels of $\theta < 90°$ are less than the space average level and for $\theta > 90°$ they are somewhat above it. For a little higher frequencies, 500 Hz - Figure 18, the directivity is nearly the same for all angles with an average variation of 2 to 3 dB. A large change occurs in the directivity of 1000 Hz. Figure 19 illustrates showing that the maximum intensity of this source of noise is near 120°, especially for microphones 2, 3, and 6. Directly under the flight path, microphone 1, the maximum noise occurs near 100°. An explanation for this change is not readily apparent. This strong directivity disappears at somewhat higher frequencies. In Figure 20 the directivity indices for 1600 Hz reveal that radiation

patterns at this frequency are much flatter than at 1000 Hz. At 2000 Hz, Figure 21, the strong directivity appears again. For microphone 2 there is an 18 dB increase in the level going from 30 degrees to 140 degrees. Again going to a higher frequency, the radiation patterns flatten as seen in Figure 22 for a frequency of 4000 Hz. Since the frequency of the highly directive sources were a multiple of each other, 1000 Hz and 2000 Hz, it is suspected that there is only one source with a harmonic or subharmonic showing up.

In order to make comparisons to data in the literature, the overall frequency level directivity plots were needed. Figure 23 shows the plots for each microphone. The general trend of increasing levels with increasing angle is readily noted. All of the microphones (except 7) show essentially the same pattern. The reason for the variation in the results from microphone 7 is not readily apparent. The results from microphone 7 for the other two flights agree well with the other results.

The directivity pattern for a measurement location directly under the flight path has been studied by several investigators (References 9, 12, 13). In most references the radiated flyover noise directly under the flight path was assumed to have the directivity of a dipole oriented normal to the flight path. However, in Reference 12 Munson showed that flyover data from a clean configured DC-10 do not agree with a simple lift dipole model. A new model for the directivity was developed which consisted of 2 dipoles, a lift dipole oriented parallel to the lift vector and a drag dipole oriented paralled to the drag vector. A sketch of both models is shown in Figure 24. The equation describing his model is

$$OAL_p = 10 \log\left[\frac{V^6}{16 \pi^2 U_o^2 (1 - M_o)^4 R^2} (K_L \sin^2\theta + K_D \cos^2\theta + K_{LD} \sin\theta \cos\theta)\right] \qquad (50)$$

The DC-10 data were used to evaluate the coefficients giving

$$K_L = 8.48X10^8 \quad sec^4/ft^2$$
$$K_D = 5.97X10^8 \quad sec^4/ft^2 \qquad (51)$$
$$K_{LD} = 3.46X10^8 \quad sec^4/ft^2$$

for the clean configuration. His data agreed well with the 2-dipole model. The glider data was compared to both models. The equation used in the comparison for the simple lift dipole model is

$$OAL_p \approx 10_{log} (\sin^2\theta) \qquad (52)$$

and for the 2-dipole model is

$$OAL_p \approx 10 \log[7.88 \sin^2\theta + 5.55 \cos^2\theta - 3.22 \sin\theta \cos\theta] \qquad (53)$$

The convective amplification and spherical divergence terms in equation 50, $(1-M)^{-4}$ and R^{-2}, respectively, were not used in equations 52 and 53 because corrections were applied to the glider data accounting for these variations. The measured directivity derived from microphone 1, directly under the flight path, is shown in Figure 24. The 2-dipole model was matched to the data at 100° and the single lift dipole model was matched at 90° to give the best fit. The comparison definitely substantiates Munson's 2-dipole model. Thus, it appears that the best model for the directivity of the total non-engine acoustic radiation from clean configured aircraft is the combination of a lift and drag dipole.

SECTION IV

TOTAL RADIATED ACOUSTIC POWER

One of the objectives of this effort was to determine the total radiated acoustic power from the Schwiezer 2-32 glider. The necessary methodology was developed in Section II with the results presented in equation 43. This equation was applied to the three glider flyovers selected for analysis. The power level for each one-third octave band as well as the overall power level was obtained. The results for each flight were averaged into one spectrum since they showed little variation. The average spectrum is shown in Figure 25. Most of the acoustic energy is concentrated in the one-third octave band centered at 1250 Hz. However, the lower frequencies, less than 200 Hz, tend to have high levels also. The average overall level of the three flights is 106 dB.

If one considers the directivity results of paragraph d of Section III, the question arises as to how much accuracy was gained in using the detailed methodology of Section II. Since the directivity revealed that the levels are fairly uniform in most directions, the overall radiated power can be calculated from one flyover measurement using the equation

$$L_W = \bar{L}_p + 20 \log R + 11 \qquad (54)$$

The necessary assumption is that the one measured level is approximately equal to the space average sound pressure level $\bar{L}_p$. This was assumed for the glider flyovers and the acoustic power was determined. Since the measured levels from the three flights were within 3 dB, averaged levels were used. The first level was obtained from the average of the maximum levels recorded

from the three flights analyzed. This yielded an overall power level of 107 dB. The other level was the average of the three values from microphone one when the glider was directly overhead. The overall acoustic power from this level is 105 dB. The first value is one dB greater than the result from equation 43 and the second one is one dB less than the result from equation 43. Thus, the true space average sound pressure level is between the two levels. It has to be concluded that the significant amount of effort required to utilize equation 43 to calculate the total acoustic power is not warranted since one single measurement and equation 54 give the overall power within 1 dB of the average level. However, this statement only applies to a clean configured aircraft. If one tries to determine the total acoustic power utilizing the simplified approach for a dirty configuration, i.e., landing gear down, open cavities, flaps, etc., it will not give the true power because the directivity pattern would be considerably different from the clean configuration. Thus, the methodology developed in Section II is still useful since most aircraft during runway approach are in a dirty configuration.

A comparison of the glider power level to other clean aircraft flyover levels is desired. Figure 26 displays sound power levels from 18 different sources. The range of size, or weight, is very large. For example, the 747 weighs 710,000 pounds and the small remotely piloted vehicles weigh only 9 pounds. The owl weighed only 1.5 pounds. The data are plotted as overall power level versus flight velocity in meters per second. An arbitrary V^6 line is shown in the figure. The data, in general, follows this line which substantiates the dipole radiation pattern discussed in Section III.

Several normalization expressions have been proposed in the literature. The most promising ones were evaluated and are presented here. Numerous other

expressions were investigated but only a few of these are presented. In Reference 10 an extensive regression analysis was performed to determine the parameters, and their exponents, which best normalize their data. The result was S/AR^4 where S is the wing area and AR is the aspect ratio. All of the available data were normalized with this expression with the result shown in Figure 27. For the data which were used in Reference 10 the expression appears good but for the other data the expression is not very good. In fact, the F-106 level is approximately 30 dB too low. In Reference 3 the weight of the aircraft was used to normalize the data. All of the available data were plotted using weight as the basis of comparison. Figure 28 shows the comparison. Just normalizing the acoustic power levels with weight does a surprisingly good job of collapsing the data. Even the F-106 result is within 2 dB of the other data. The lightest noise source, the owl, is seen to be somewhat above the trend. Thus, other normalizing parameters were investigated to determine if one could be found to collapse all of the data.

One of the parameters investigated was the wing span b. It is revealed in Figure 29 that b does a fair job of normalizing the data. Another parameter that gave reasonable collapse is S/AR. Figure 30 indicates that S/AR does well for all the sources except the F-106. It is about 13 dB below the trend. The best normalizing parameter which resulted from this extensive investigation was S, the wing area. This is displayed in Figure 31. Even the F-106 level is only 7 dB below the trend. The owl level is somewhat above the trend but this is not surprising since it was not expected that the owl's acoustic power level would follow exactly the same trend as aircraft.

The large amount of scatter in the data in the 30 to 60 m/sec range is a result of the gliders. Each of the four gliders tested display narrowband

energy at some particular frequency. The amplitude of narrowband energy varies significantly more than broadband energy, which results in significant data scatter. Essentially, none of the other sources exhibited strong narrowband energy. To eliminate the scatter from the glider results, the available data for each glider was averaged and only the averaged level was utilized in the final comparison. Figure 32 shows the averaged glider results. A regression analysis was performed on the data to determine the best fit line. Two data points were not included in the analysis: those from the owl and the F-106. They were not included because a best fit of the other data was considered more important than a best fit of all the data. This line results in a root-mean-square error of only 2.4 dB and a maximum error of 6 dB. Even the F-106 level is only 8 dB below the best fit line. In view of the very wide range of aircraft included (9 pounds to 710,000 pounds) the degree of normalization is considered very good.

The equation which describes the best fit line is given by the following expressions:

$$L_w - 10 \log S = 45.54 \log V + 26.04 \tag{55}$$

By grouping the terms equation 55 becomes

$$L_w = 10 \log (402\ SV^{4.55}) \tag{56}$$

where S is the total wing area in square meters and V is the aircraft velocity in meters per second. This equation is recommended for predicting the overall radiated acoustic power during flyover of clean configured aircraft.

As mentioned above, the owl results were not utilized in the regression analysis. Its velocity was nearly an order of magnitude less than all of the other noise sources and its acoustic power level is approximately 12 dB above the regression analysis curve. A possible explanation for this deviation is that for very low velocity flights the radiated acoustic power may not follow the same slope as for higher velocities. That is, there should be a break point at some velocity where the slope of the best fit curve increases. Justification for this break point can be found in Reference 14. Guenther found that the sound generated by low speed, small diameter rotating blades very clearly displays a break point in the data. However, since most aircraft will operate well above this velocity, no attempt was made to determine if airframe noise also has some critical velocity at which the data follows a different slope.

SECTION V

CONCLUSIONS, RECOMMENDATIONS, AND PREDICTION EXAMPLE

Methodology which enables the calculation of the total radiated acoustic power for an aircraft flyover was developed and applied to a Schweizer 2-32 glider. Application of the methodology requires flyover acoustic measurements from an array of microphones perpendicular to the line of flight. The effects of spherical divergence, doppler shift, and atmospheric absorption are accounted for. The results of the Schweizer 2-32 glider were compared to other available flyover data and an expression was derived to predict the acoustic power from any aircraft. Also, the spectrum shape recommended in the literature was modified to account for the narrowband energy observed in most flyover data. The directivity of the radiated noise was also investigated.

Based on the results of this study, the following conclusions and recommendations were reached:

1. The detailed approach used to calculate the acoustic power did not significantly (1 dB) increase the accuracy of the result over the level obtained from using the measured SPL directly under the glider and assuming a monopole source to calculate the acoustic power.

2. The directivity, in the direction of flight, agrees well with a two-dipole model where one dipole is parallel to the lift vector and the other one parallel to the drag vector.

3. The overall acoustic power level from different vehicles obeys a V^6 relationship.

4. The parameter which best normalizes the overall acoustic power level is the wing area.

5. It is recommended that future flight tests be conducted at a high enough velocity to ensure that the signal-to-noise ratio is large enough to avoid background noise problems.

To illustrate the use of the results of this effort, a sample prediction is included. The airframe noise of a clean configured 747 will be predicted. Knowing the wing area, 511 m^2, and assuming an approach velocity of 130 m/s, the first step is to determine the overall radiated acoustic power. Either Figure 32 or equation 56 is utilized to do this. From Equation 56 an overall acoustic power of 149 dB is obtained. Next, for a flyover altitude of 150 m, equation 48 is used to obtain the SPL directly beneath the aircraft. This comes out to be 94 dB. The last step is to determine the spectral content of the flyover noise. Assuming a mean wing thickness of .46m and with Figure 16 the flyover noise spectrum was determined. The final result is shown in Figure 33. This is the one-third octave band spectrum that would be measured when a clean configured B-747 is directly overhead at 150m and flying at 130 m/s.

REFERENCES

1. Smith, D.L., et al, "Measurements of the Radiated Noise From Sailplanes," TM-70-3-FDDA, July 1970.

2. Healy, G.J., "Aircraft Far-Field Aerodynamic Noise -- Its Measurement and Predictions," AIAA Paper 75-486, March 1975.

3. Putnam, T.W., Lasagna, P.L., and White, K.C., "Measurements and Analysis of Aircraft Airframe Noise," AIAA Paper No. 75-510, March 1975.

4. Gibson, J.S., "Non-Engine Aerodynamic Noise Investigations of a Large Aircraft," NASA CR-2378, October 1973.

5. Smith, D.L., et al, "Test Report on Measurements of the Radiated Noise From a Schweizer 2-32 Sailplane With and Without a Wing Mounted Multi-Start Assembly," AFFDL/FYA-73-5, May 1973.

6. Goldstein, M.E., "Aeroacoustics," NASA SP-346, 1974.

7. Harris, C.M., "Absorption of Sound in Air Versus Humidity and Temperature," NASA CR-647, January 1967.

8. Paterson, R.W., P.G. Vogt, M.R. Fink, and C.L. Munch, "Vortex Noise of Isolated Airfoils," Journal of Aircraft, Vol. 10 No. 5, May 1973.

9. Hardin, J.C., et al, "Prediction of Airframe Noise," NASA TN-D-7821, February 1975.

10. Healy, G.J., "Measurement and Analysis of Aircraft Far-Field Aerodynamic Noise," NASA CR-2377, December 1974.

11. Revell, J.D., et al, "Methods for the Prediction of Airframe Aerodynamic Noise," AIAA Paper 75-539, March 1975.

12. Munson, A.G., "A Modeling Approach to Nonpropulsive Noise," AIAA Paper No. 76-525, July 1976.

13. Paterson, R.W., and R.K. Amiet, "Acoustic Radiation and Surface Pressure Characteristics of an Airfoil Due to Incident Turbulence," NASA CR-2733, September 1976.

14. Guenther, D. A., "An Investigation of the Sound Generated by Low Speed, Small Diameter Rotating Blades," PhD Dissertation, The Ohio State University, 1974.

FLIGHT NUMBER	VELOCITY fps	ALTITUDE ft
29	135	118
30	137	172
31	134	148
ALL FLIGHTS	82-137	75-211

TABLE I
LIST OF FLIGHT PARAMETERS

TABLE II

LIST OF DATA ACQUISITION INSTRUMENTATION

Nr	ITEM	MANUFACTURER	MODEL Nr
10	Microphone Cartridge	B&K	4132
10	Cathode Follower	B&K	2612
10	Wind Screen	B&K	UA - 0082
10	Amplifier (1)	Intech	A - 2319
10	Amplifier (2)	Ithaco	442
1	Tape Recorder	Honeywell	7400
1	Time Code Generator	Data Metrics	SP - 105
1	Piston Phone	B&K	4220
1	Weather Instrument	Multitech	Mark II

Frequency	α - absorption dB/100m	Equation 42 Values
125	0.03	0.03
250	0.07	0.076
500	0.17	0.19
1000	0.40	0.49
2000	1.10	1.20
2500	1.41	1.66
3200	2.10	2.30
4000	3.00	3.12
5000	4.20	4.20
65% RH	51° F	

Table III Molecular Absorption Coefficients

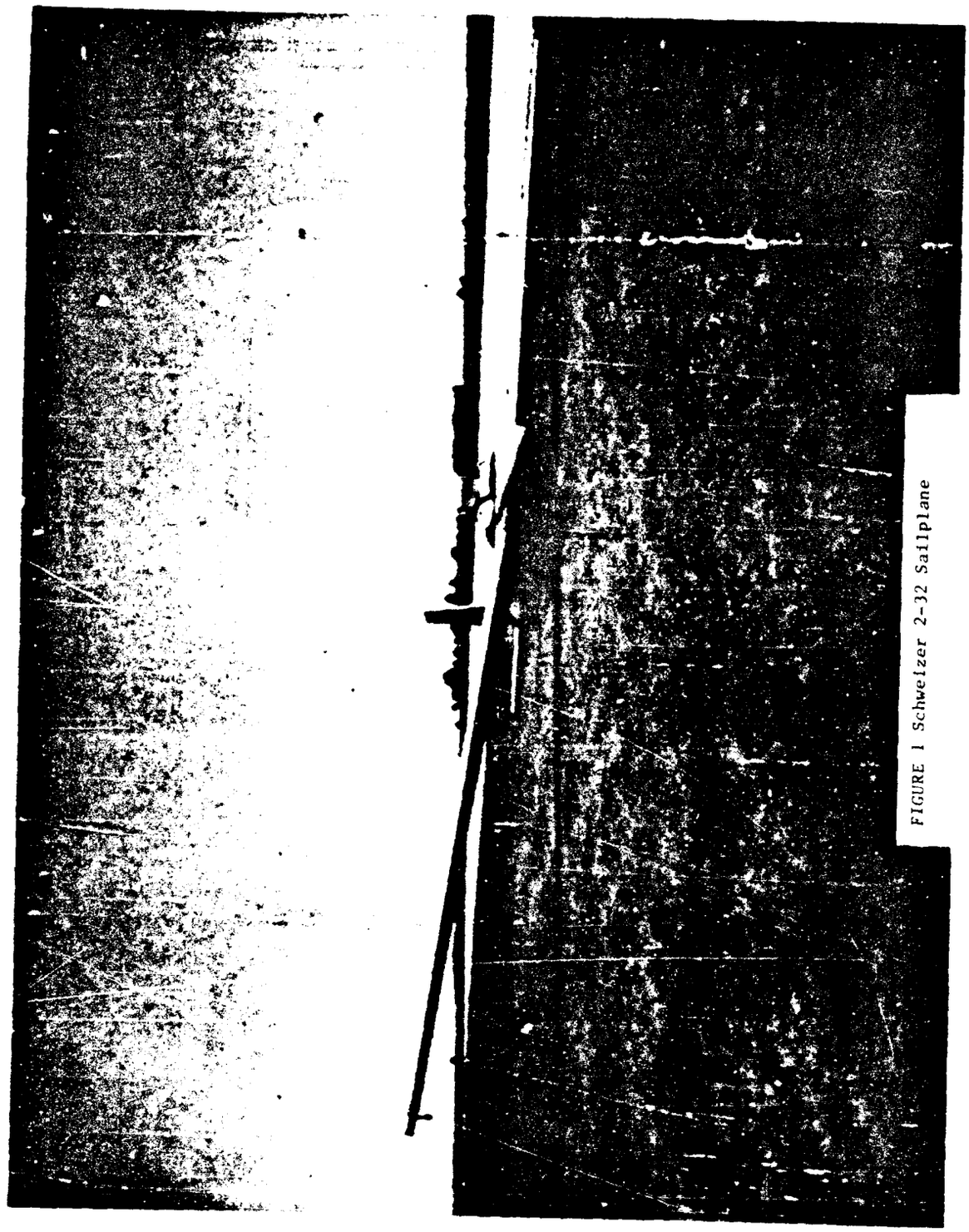

FIGURE 1 Schweizer 2-32 Sailplane

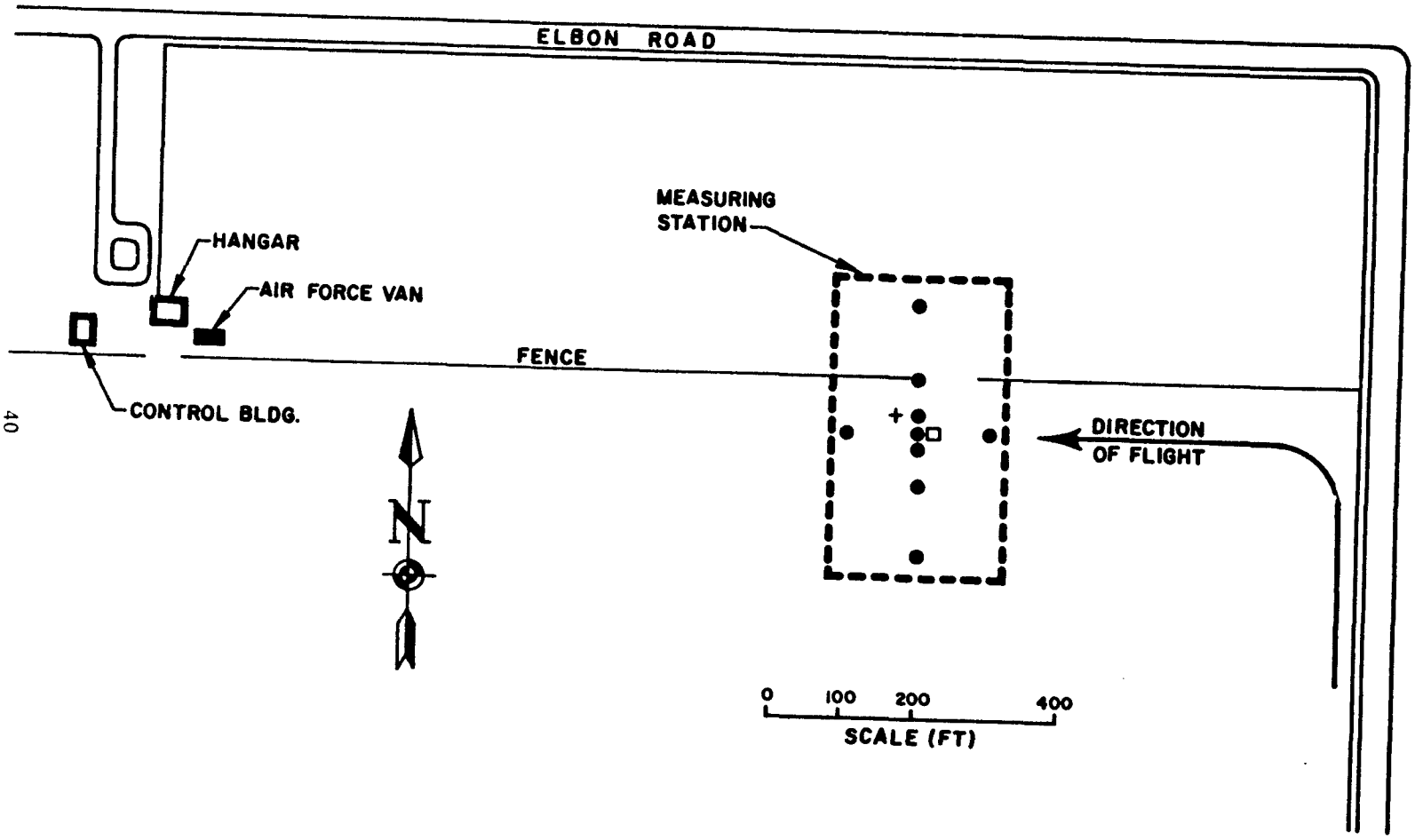

Figure 2 Test Site at Soaring Society of Dayton Airport, Waynesville, Ohio

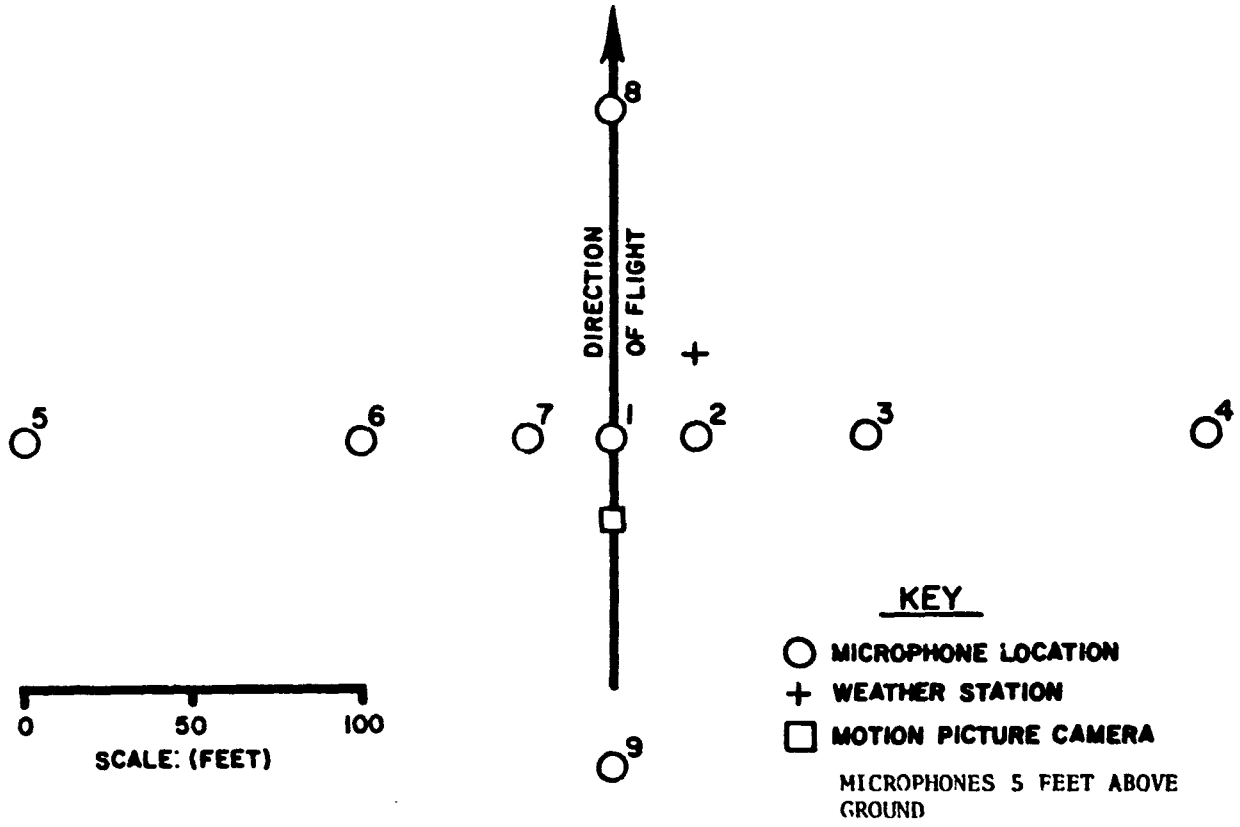

Figure 3 Measuring Station

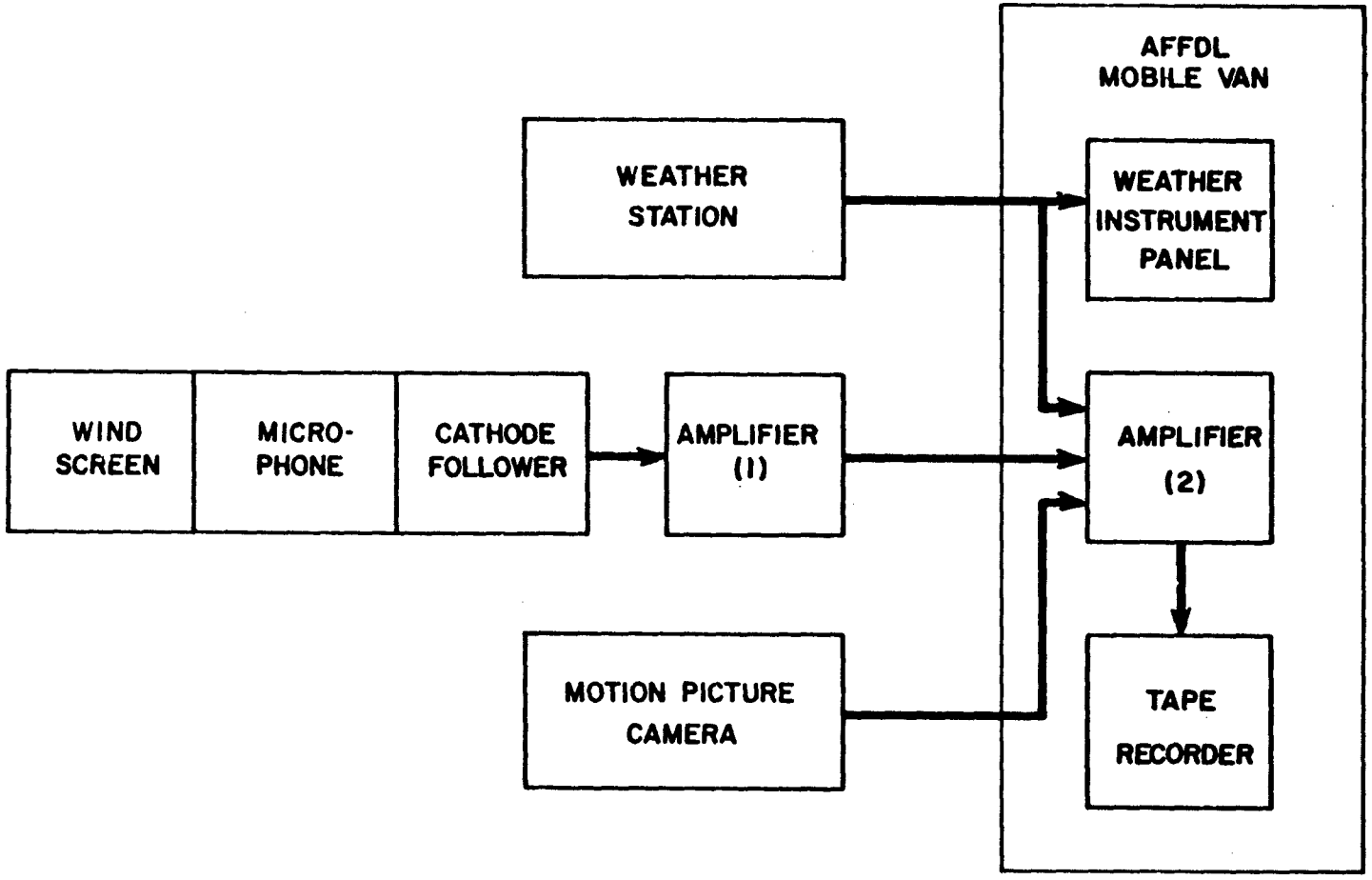

Figure 4 Block Diagram of Data Acquisition System

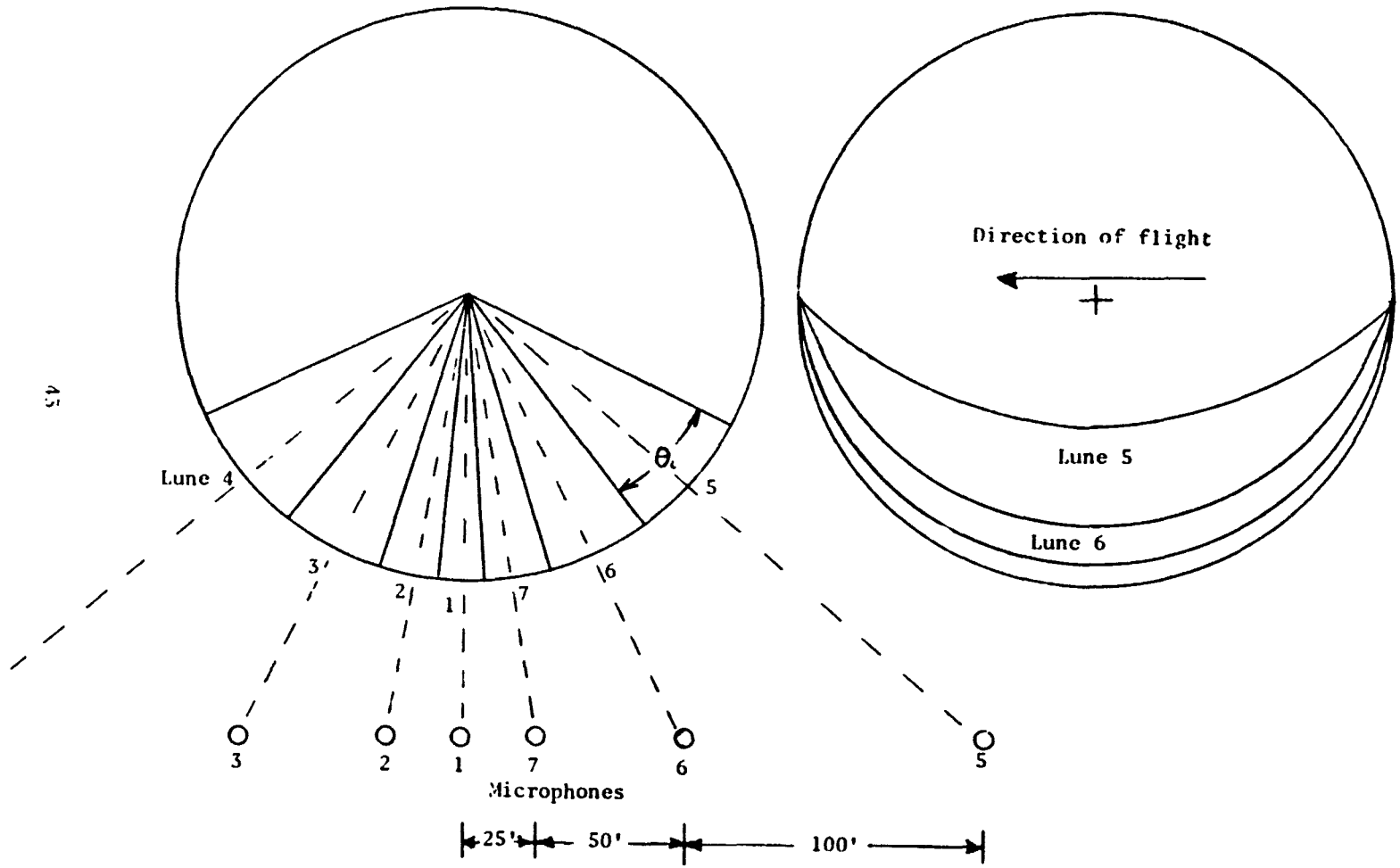

Figure 5 Microphone Locations Relative to the Imaginary Sphere

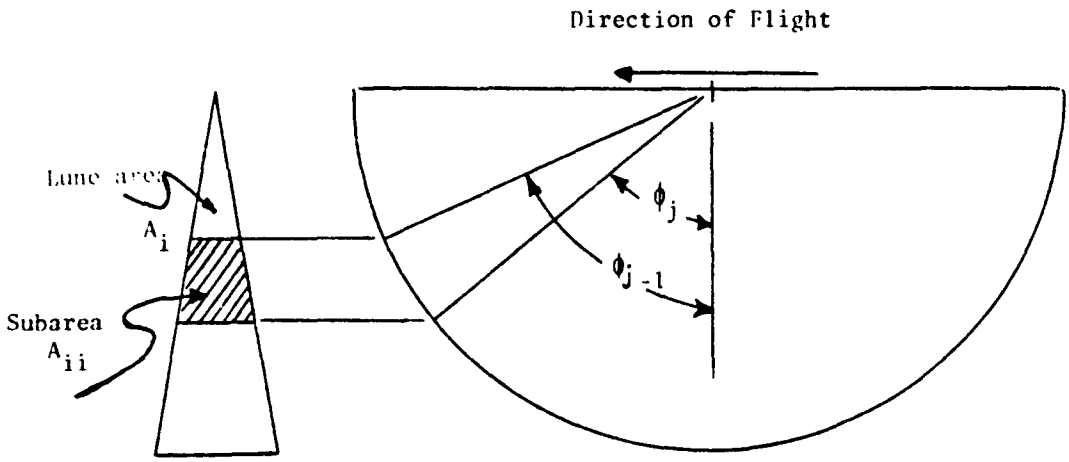

Figure 6 Illustration of Subareas

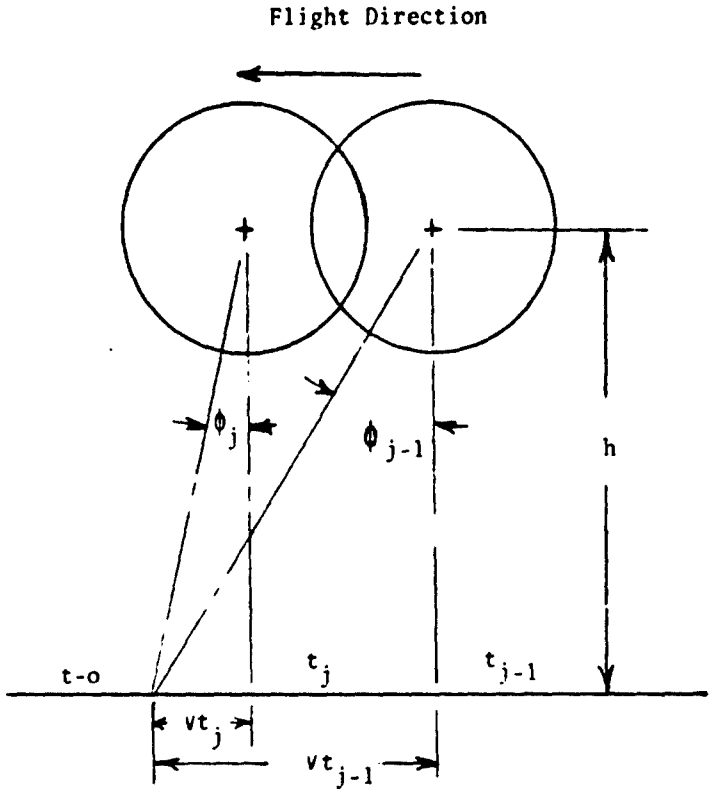

Figure 7 Sketch Showing Source at Different Times

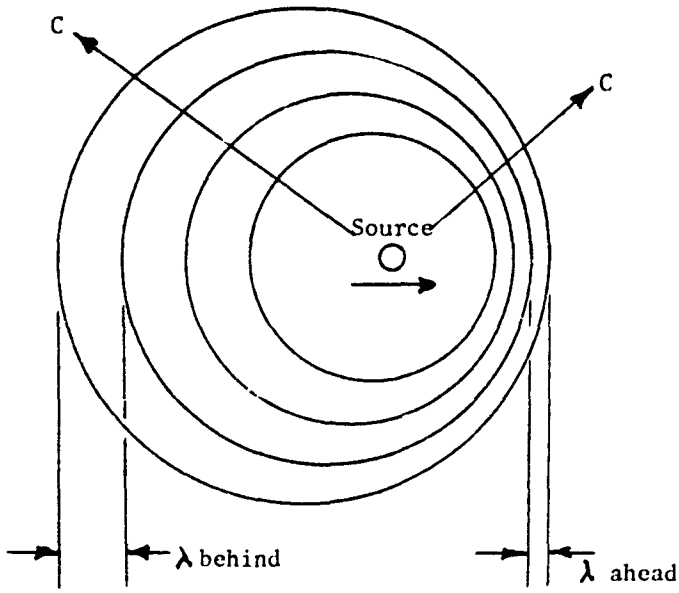

Figure 8 Moving Source Illustrating Doppler Effect

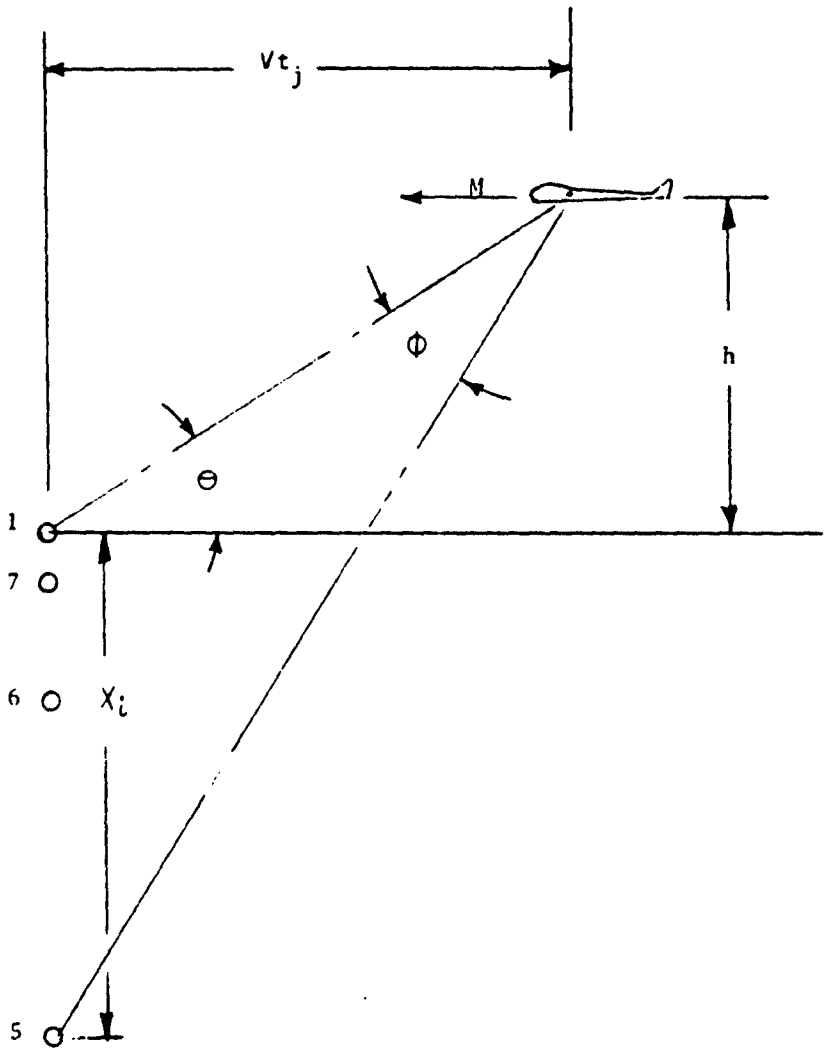

Figure 9 Determination of Relative Mach Number

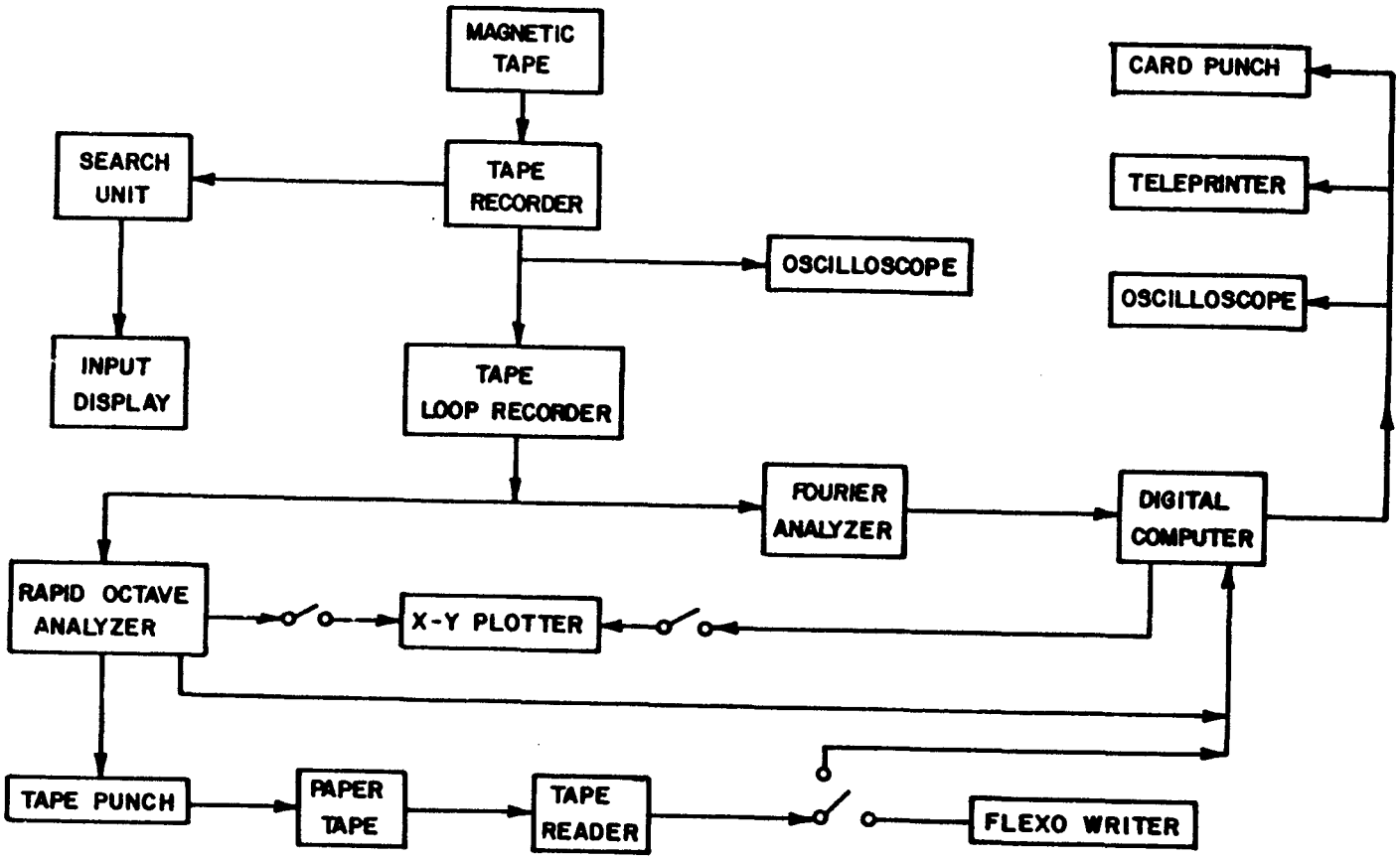

FIGURE 10 DATA REDUCTION SYSTEM

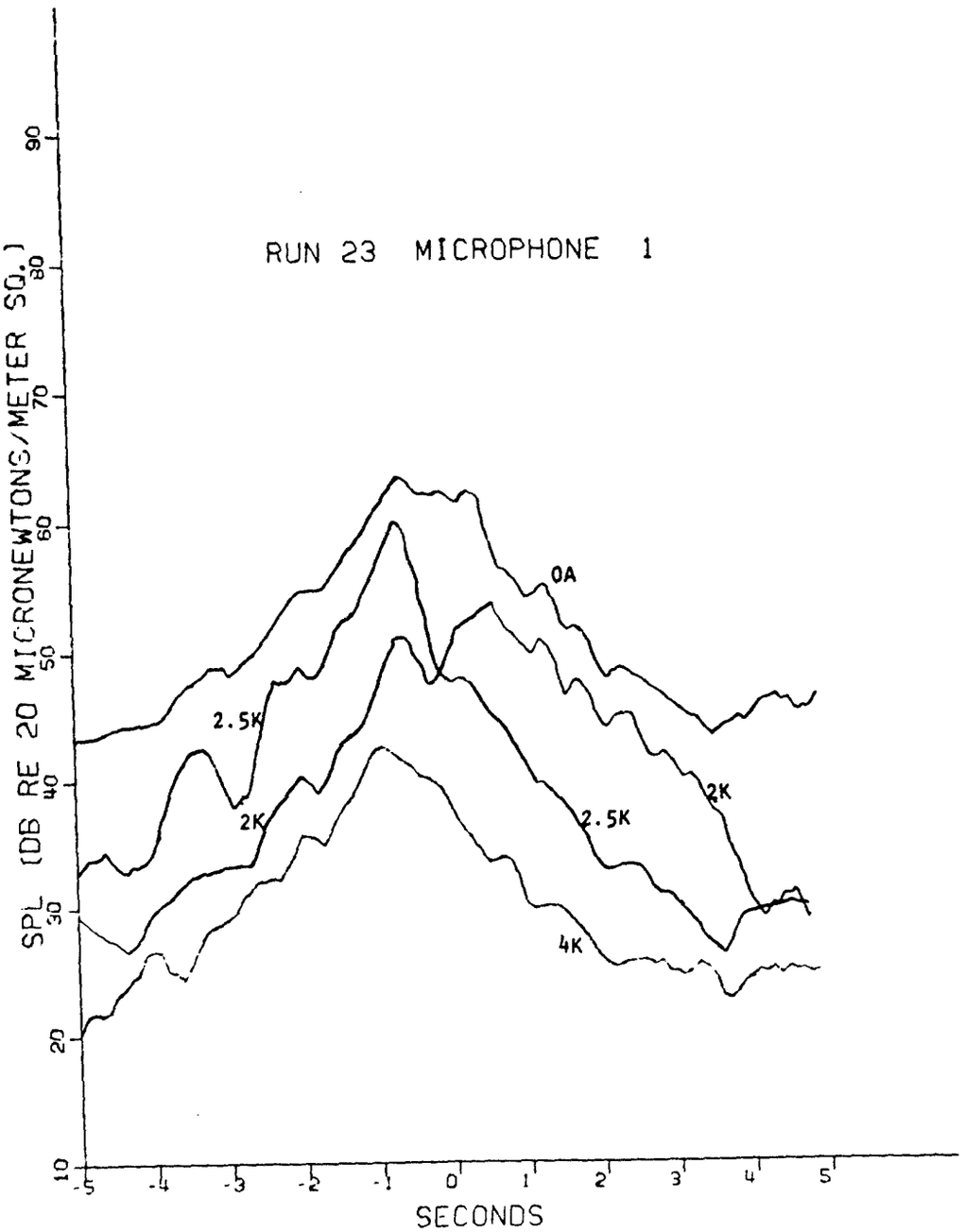

Figure 11 Time Histories for the Overall and Three One-Third Octave Band Sound Pressure Levels from Microphone 1 for an Altitude of 118 Feet and Velocity of 135 Feet per Second.

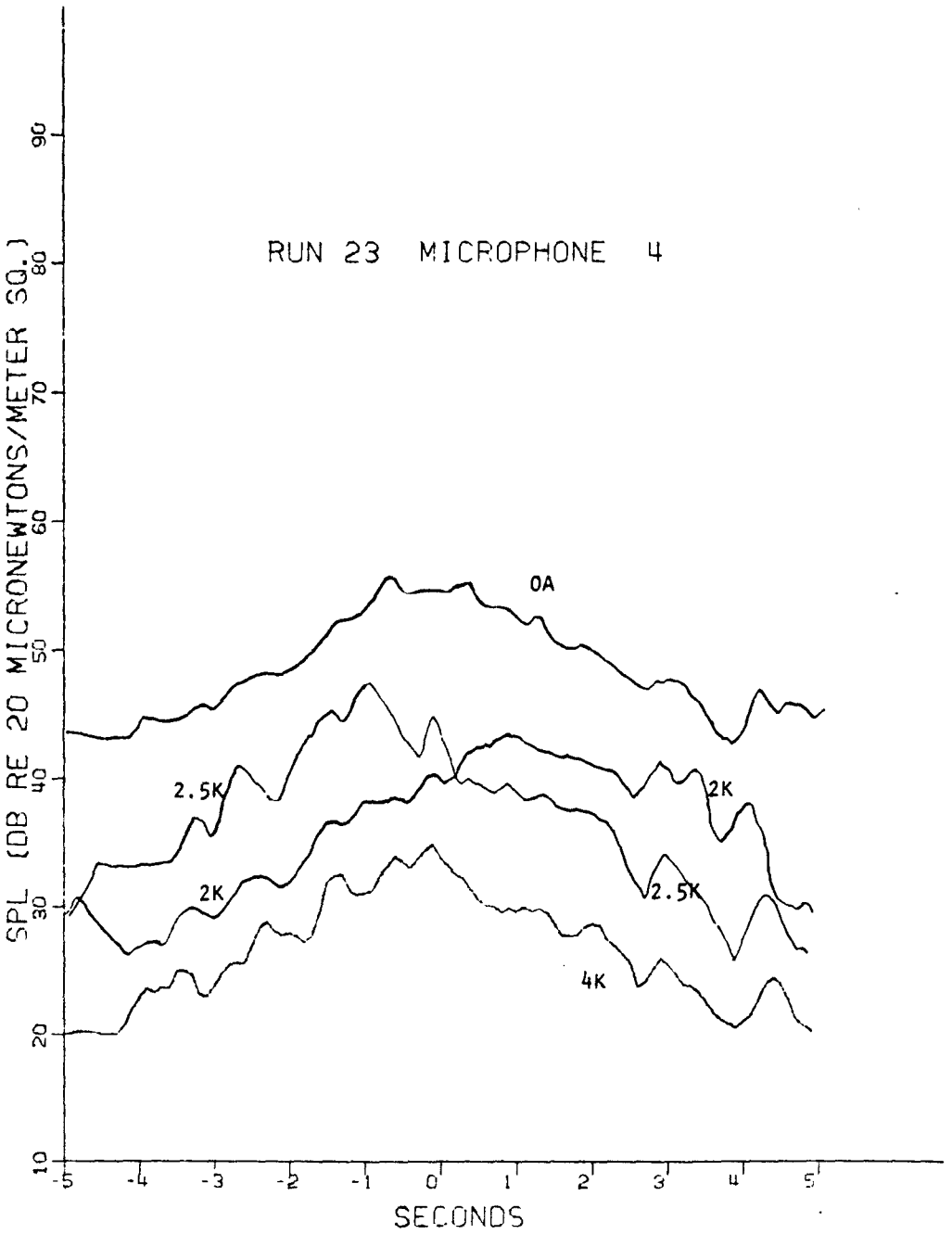

Figure 12 Time Histories for the Overall and Three One-Third Octave Band Sound Pressure Levels from Microphone 4 for an Altitude of 118 Feet and Velocity of 135 Feet per Second.

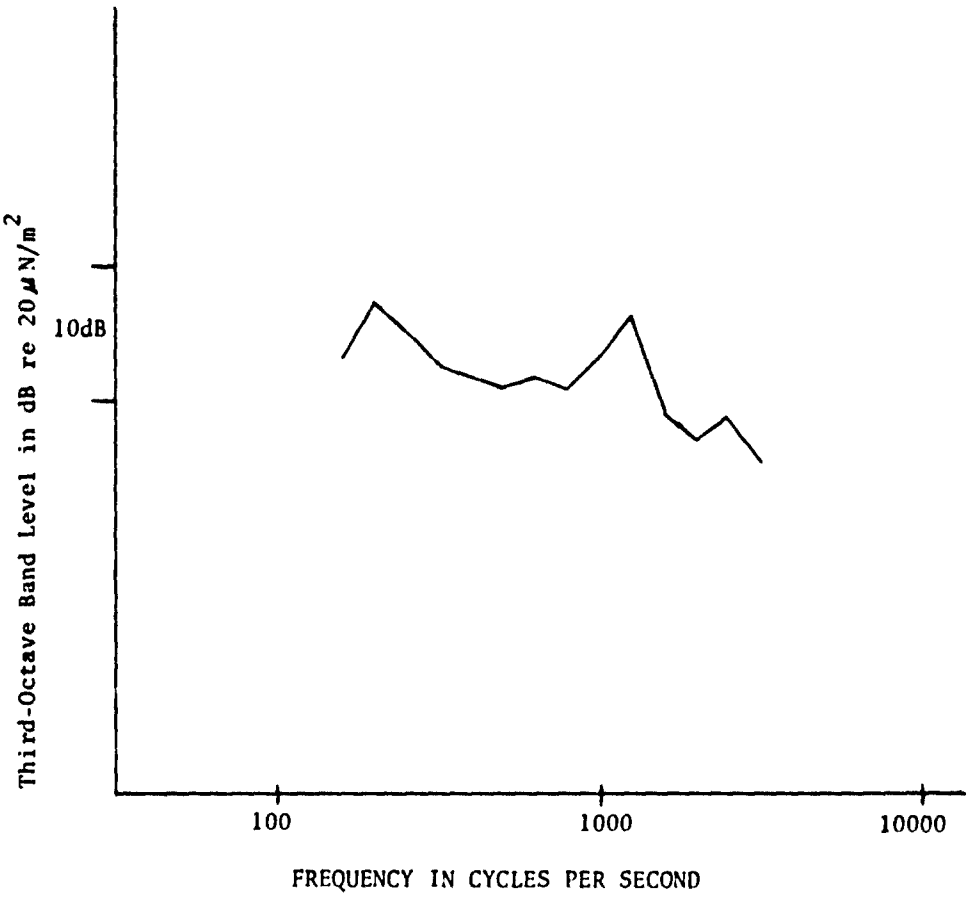

FIGURE 13 Mean One-Third Octave Band Spectra During Schweizer 2-32 Flyovers For the overhead Position

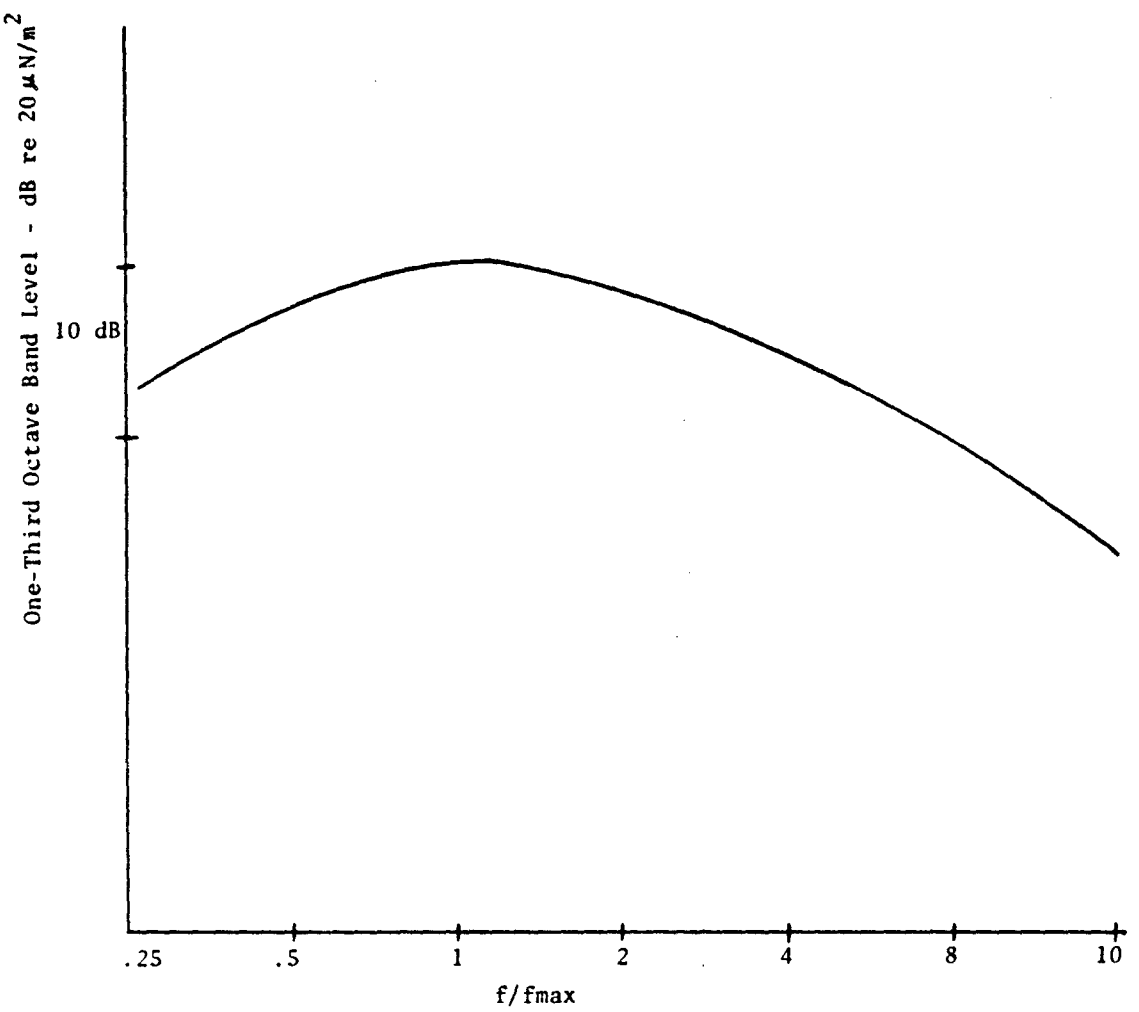

fmax = 1.3 V/t

Figure 14 One-Third Octave Band Spectrum for Clean Aircraft Flyover

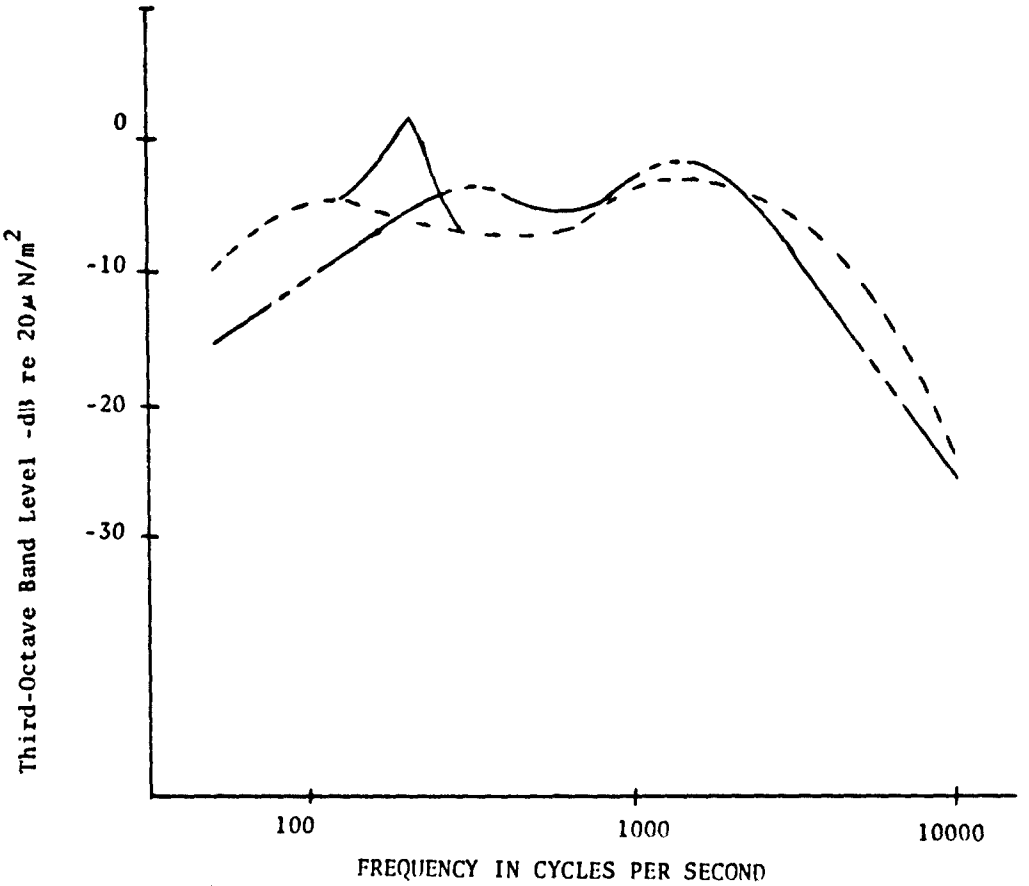

Figure 15 One-Third Octave Band Flyover Spectra for a B-747 and a CV 990 Aircraft

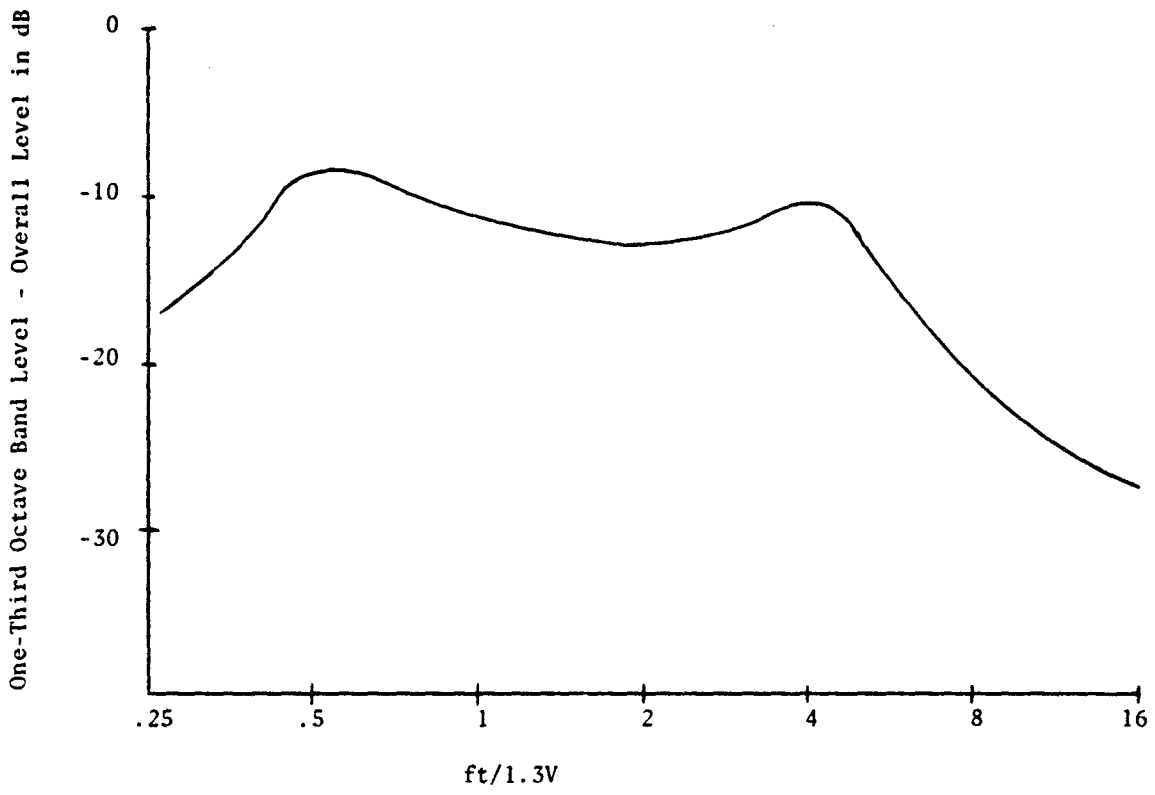

Figure 16 Modified One-Third Octave Band Spectrum Shape for Clean Aircraft Flyover

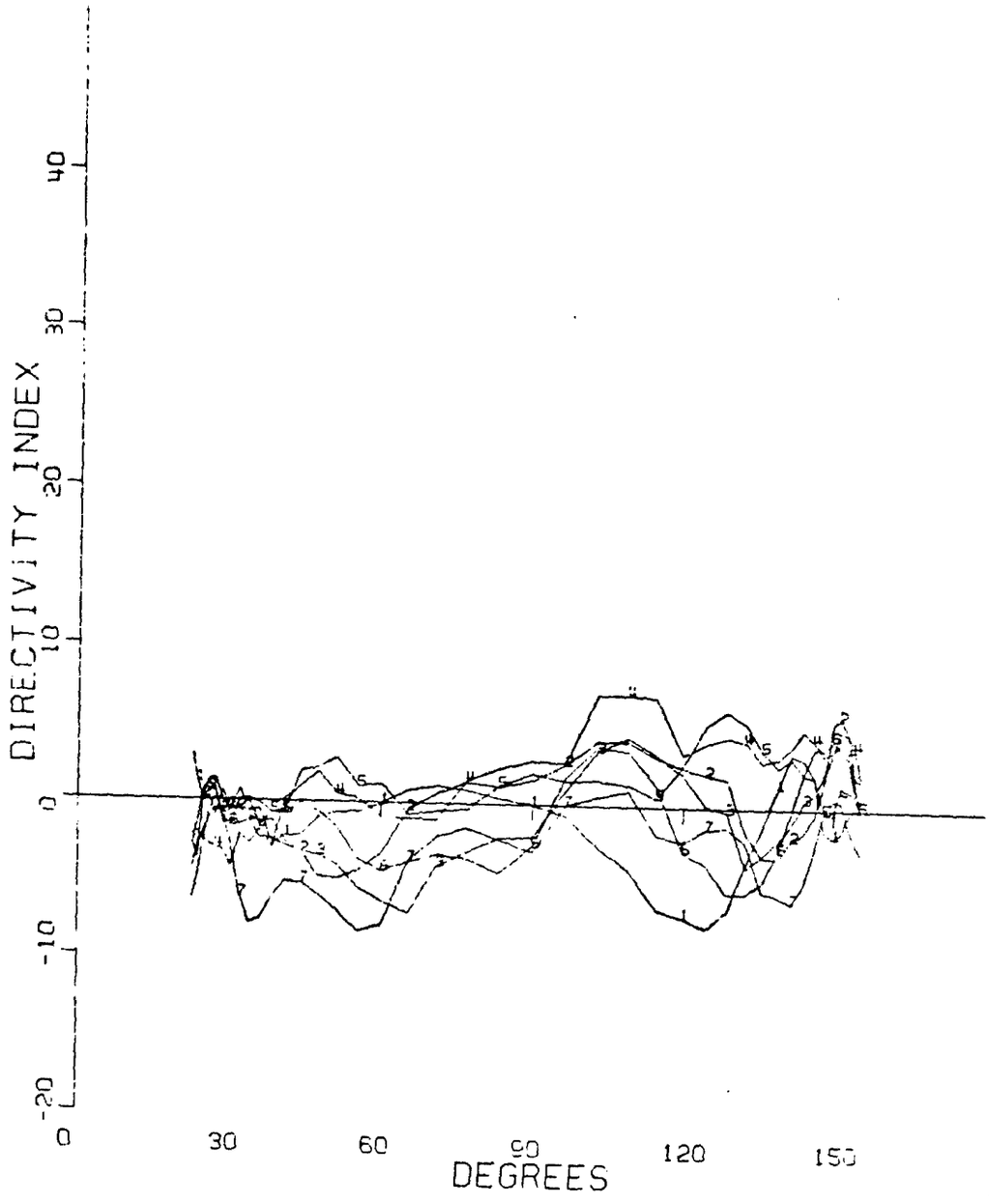

Figure 17 Directivity Indices for the 200 Hz Band

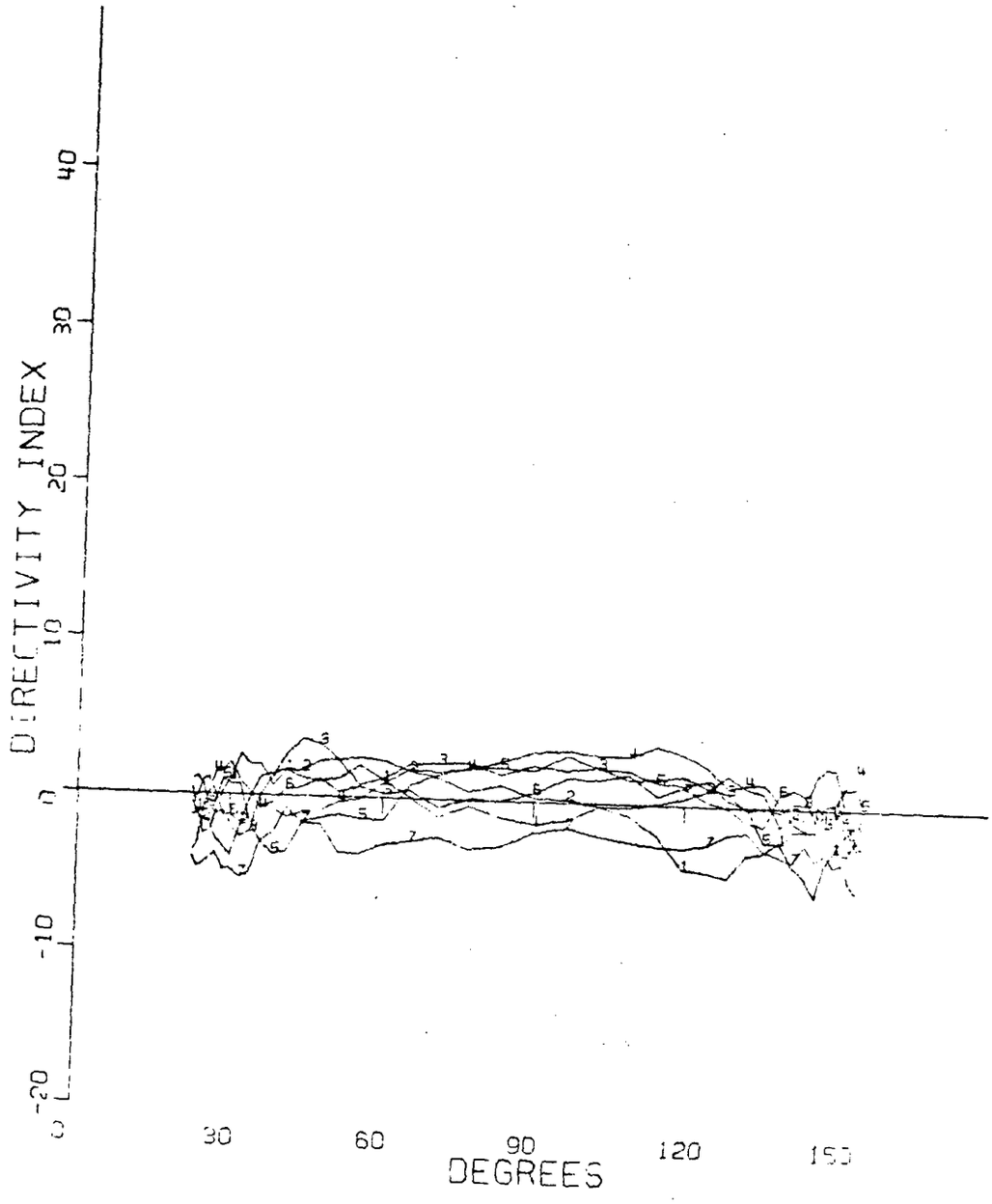

FREQUENCY 500HZ FLIGHT 23

Figure 18 Directivity Indices for the 500 Hz Band

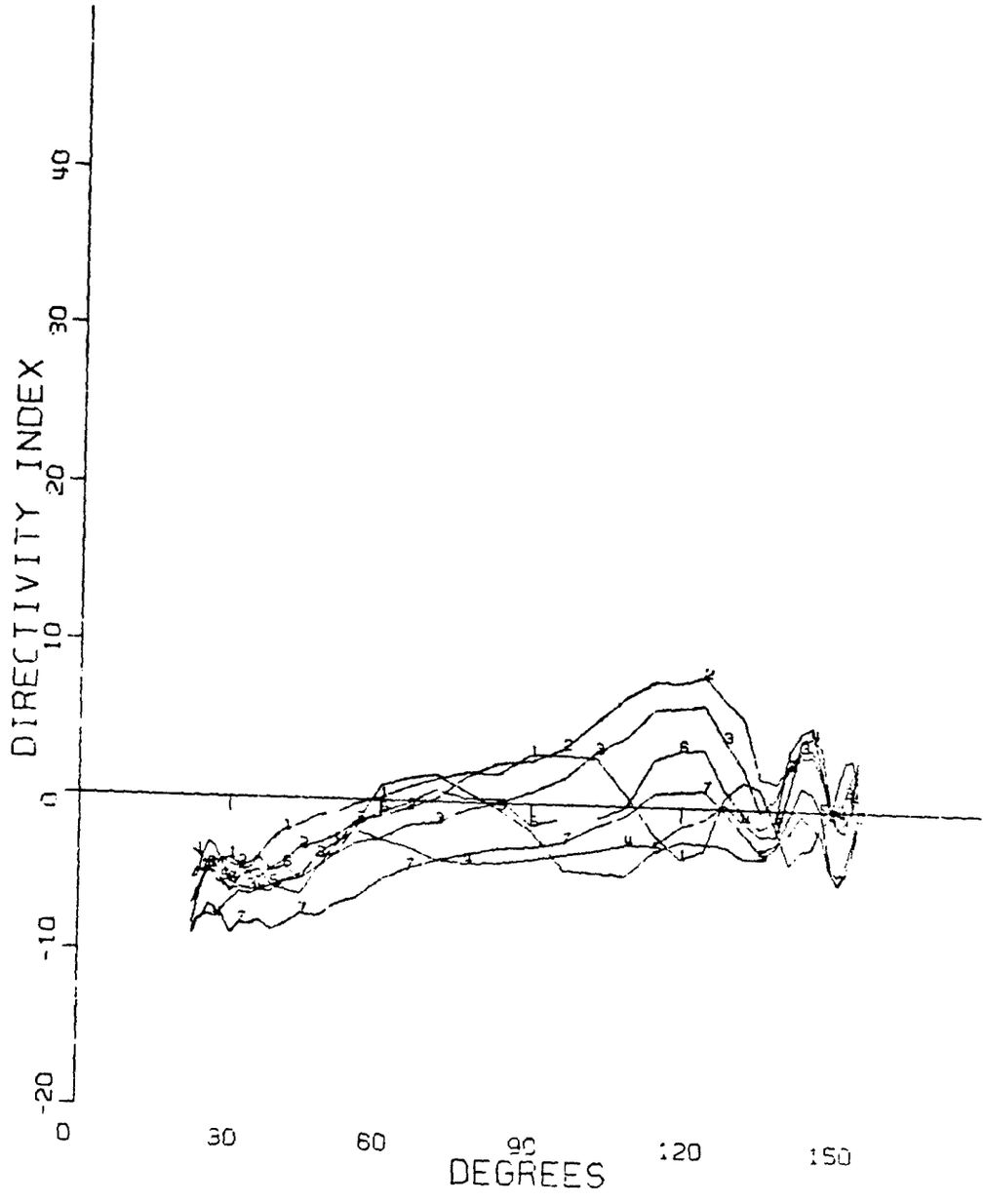

Figure 19 Directivity Indices for the 1000 Hz Band

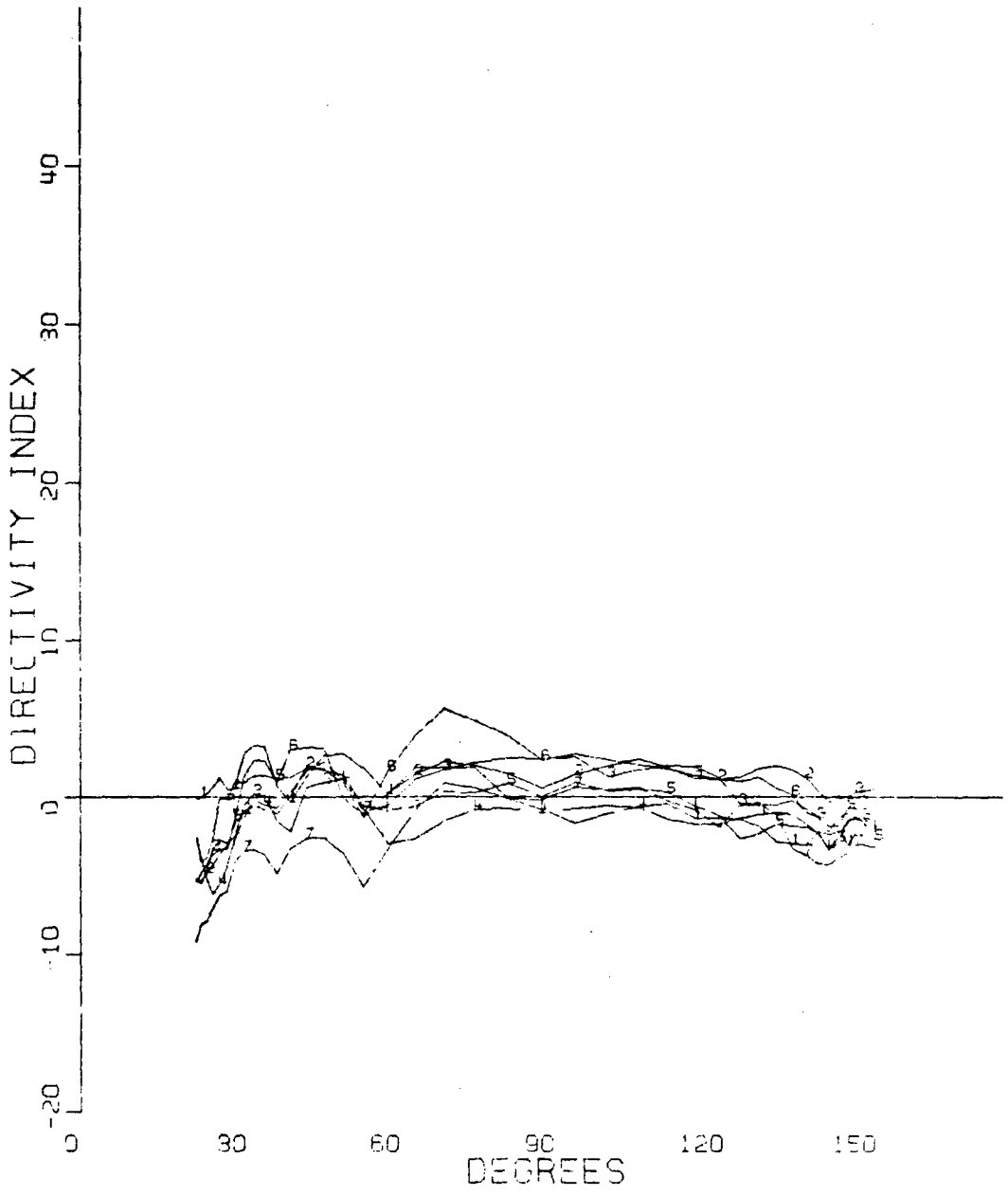

FREQUENCY 1600HZ FLIGHT 23

Figure 20 Directivity Indices for the 1600 Hz Band

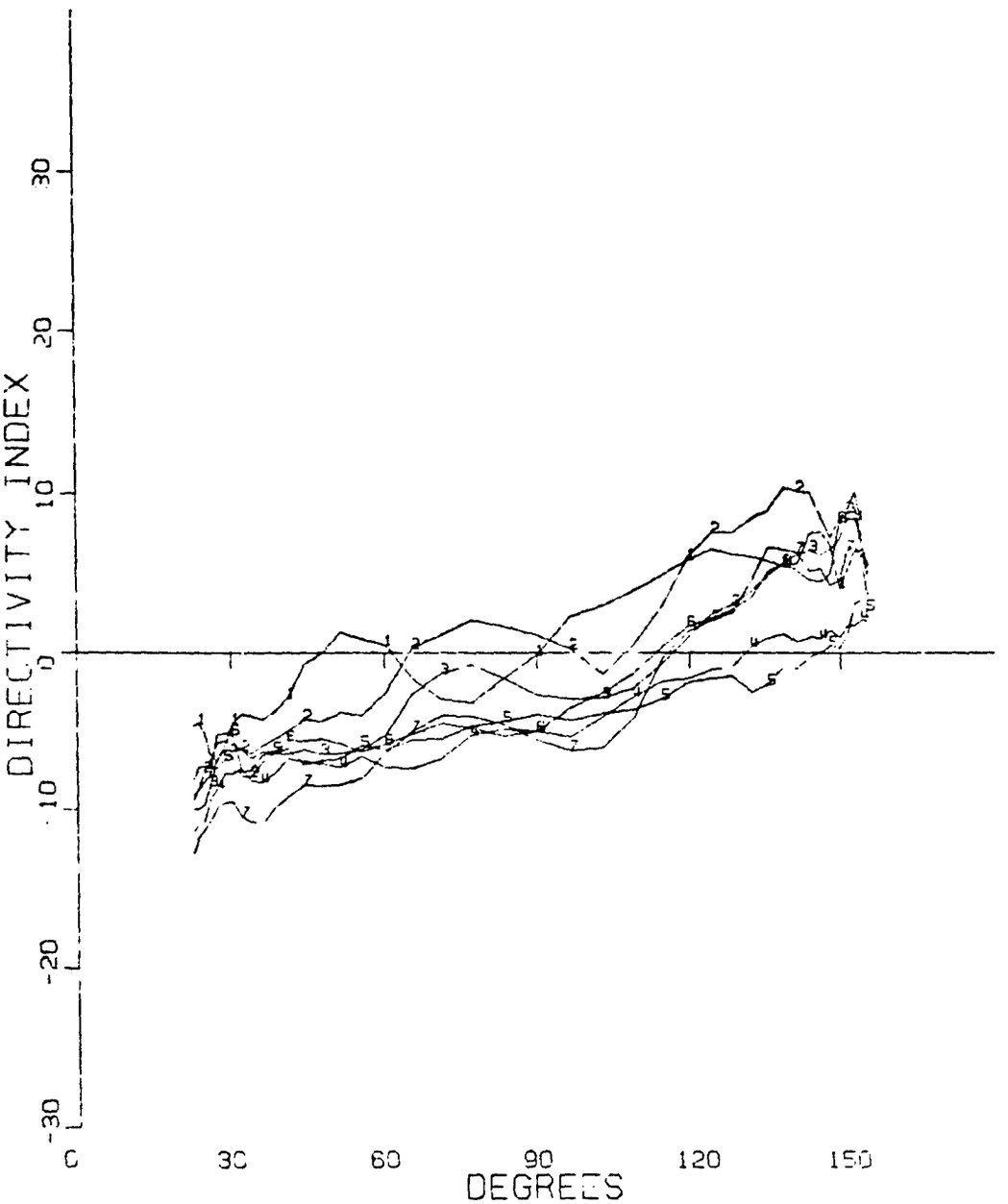

FREQUENCY 2000HZ FLIGHT 23

Figure 21 Directivity Indices for the 2000 Hz Band

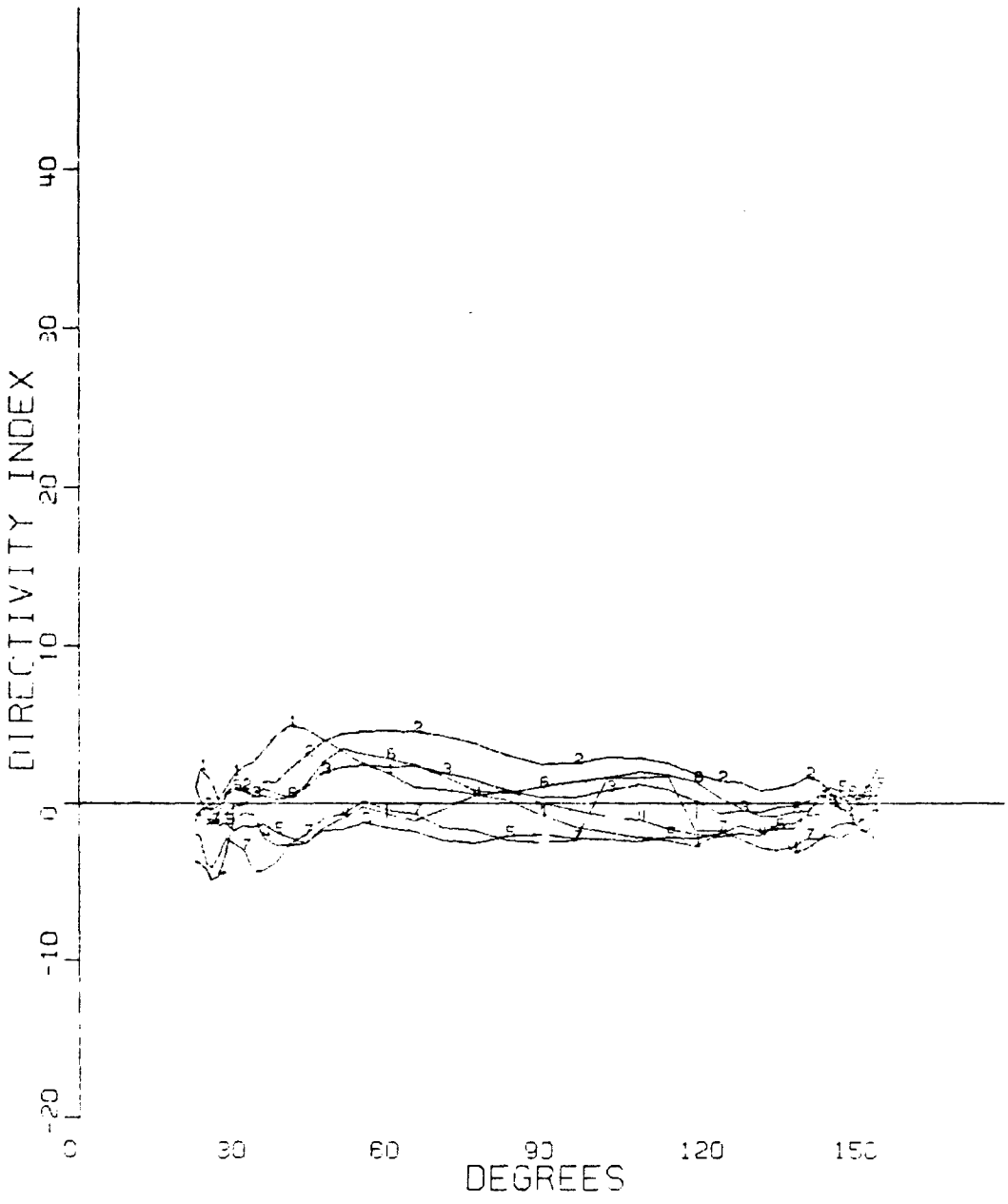

FREQUENCY 4000HZ FLIGHT 23

Figure 22 Directivity Indices for the 4000 Hz Band

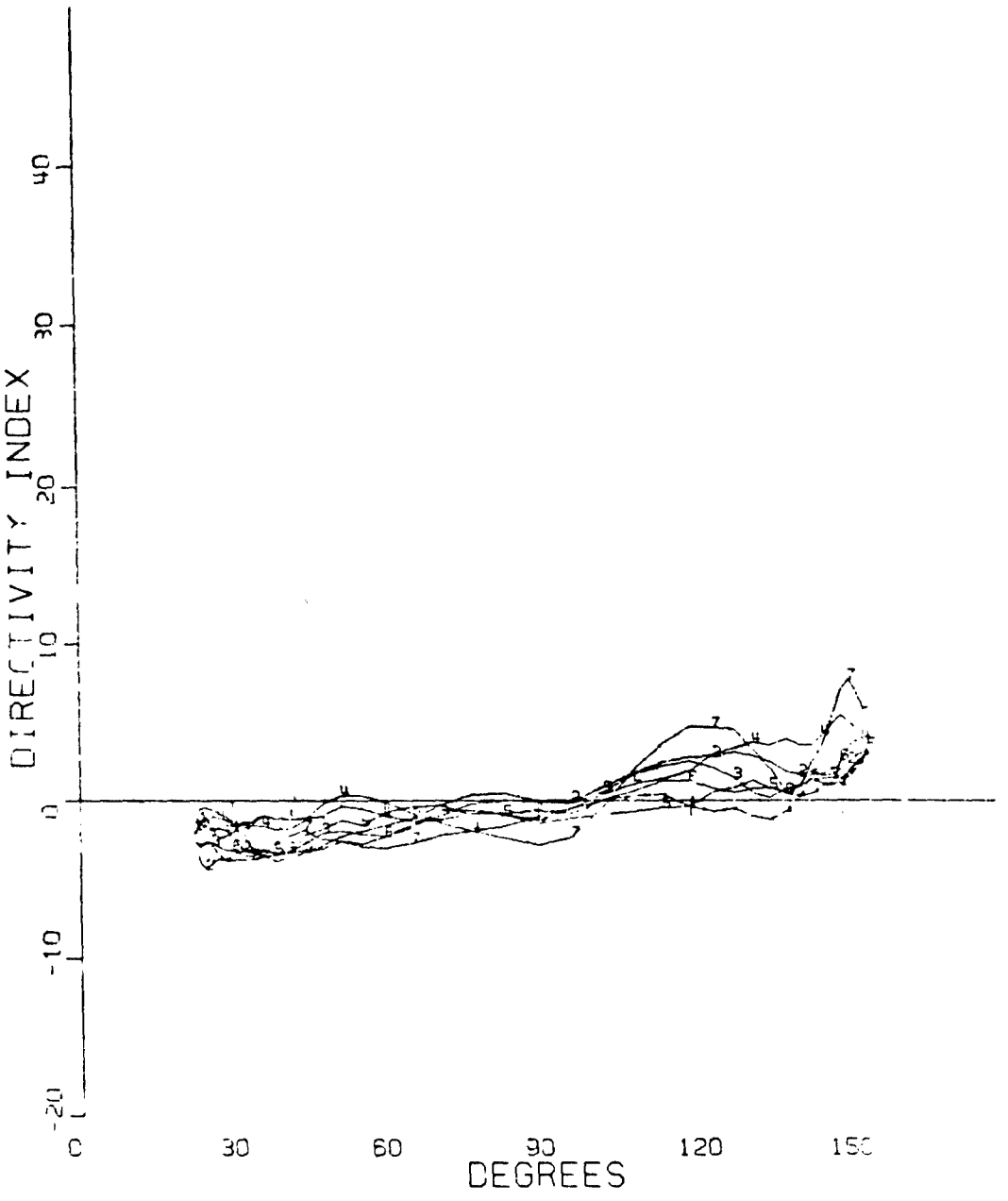

FLIGHT 23

Figure 23 Directivity Indices for the Overall Sound Pressure Level

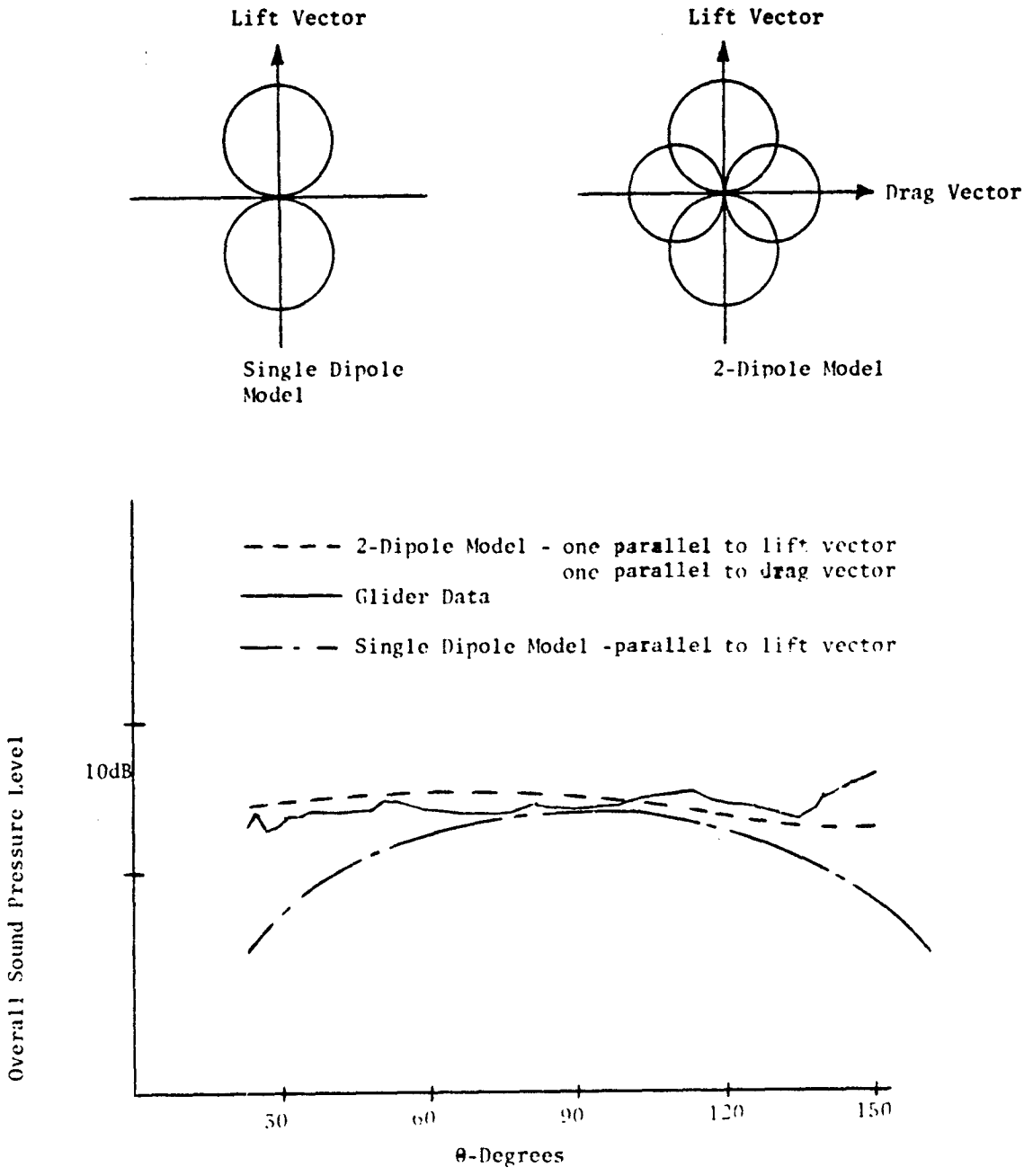

Figure 24 Comparison of the Measured Directivity Pattern to Theoretical Models

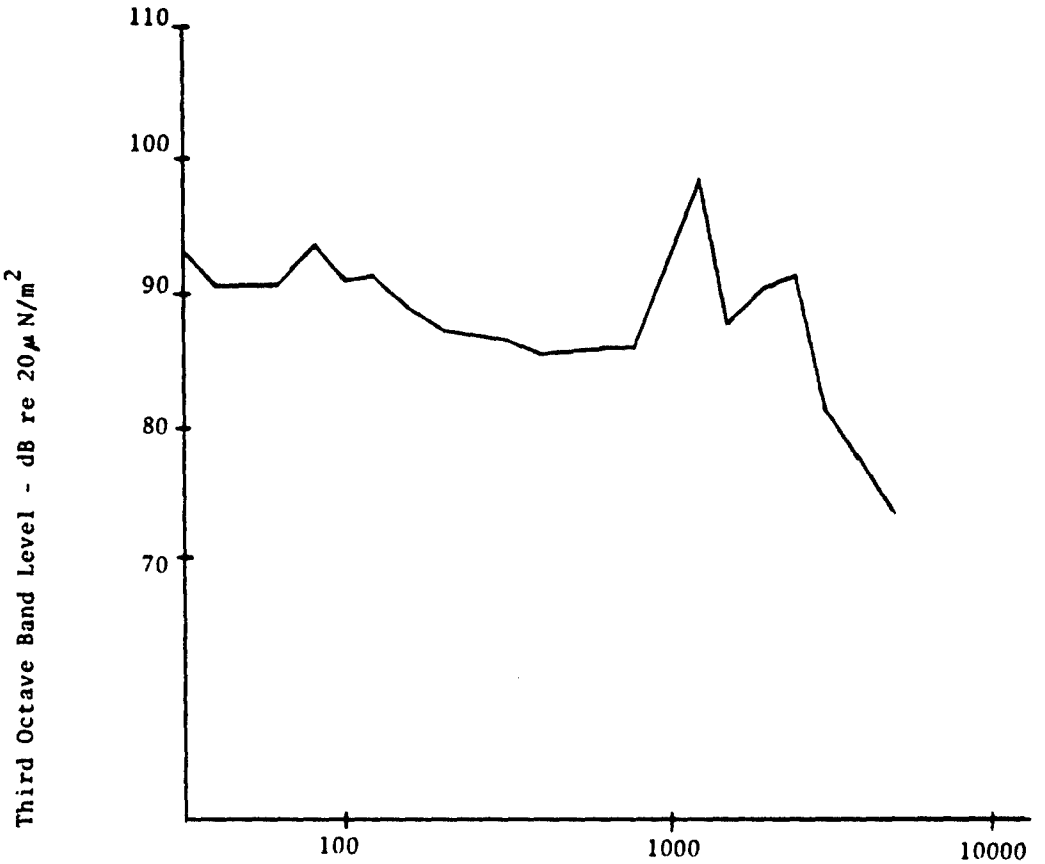

FIGURE 25 Average Total Radiated Acoustic Power from the Schweizer 2-32 Glider

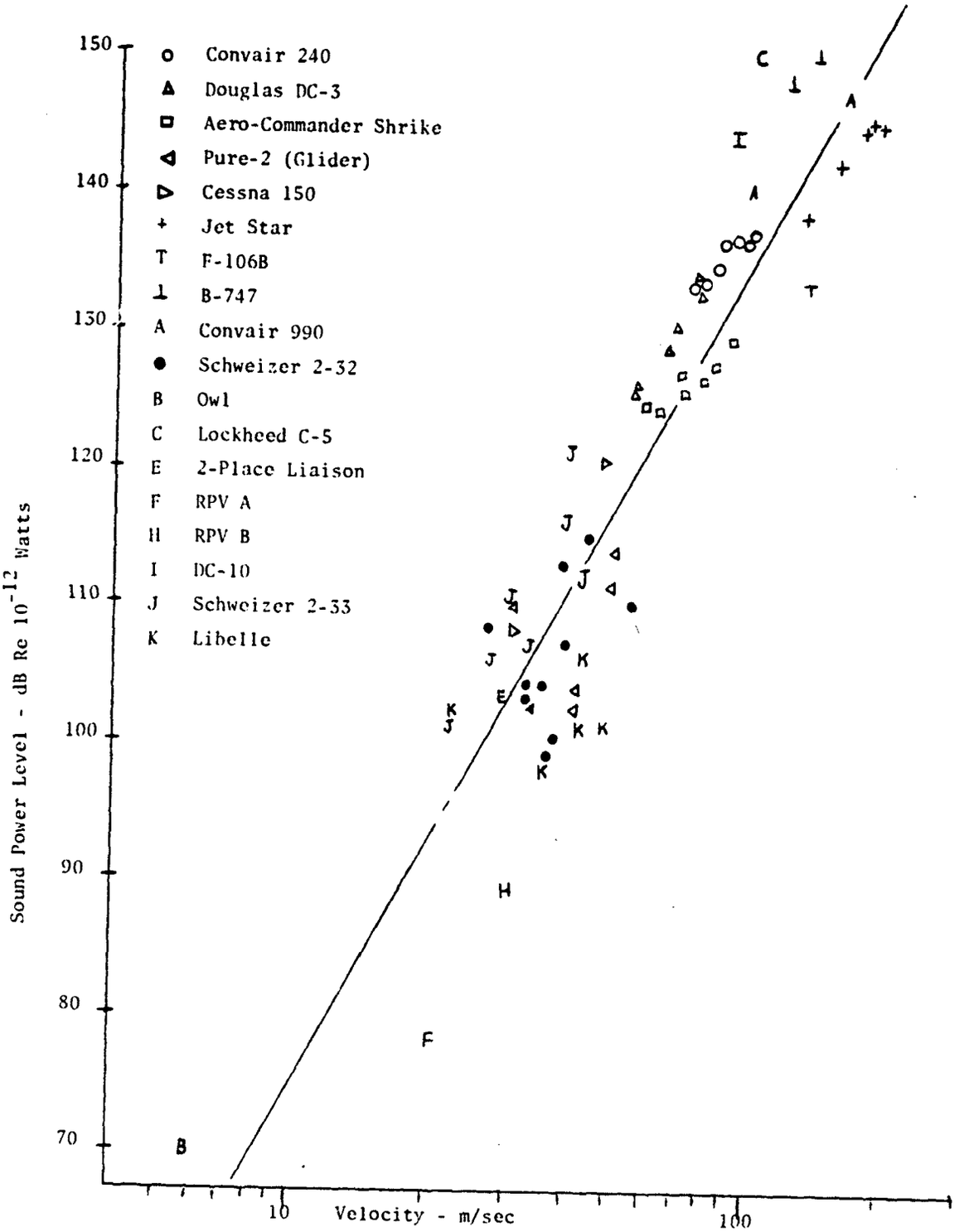

Figure 26 Clean Configured Aircraft Flyover Acoustic Power Levels Versus Velocity

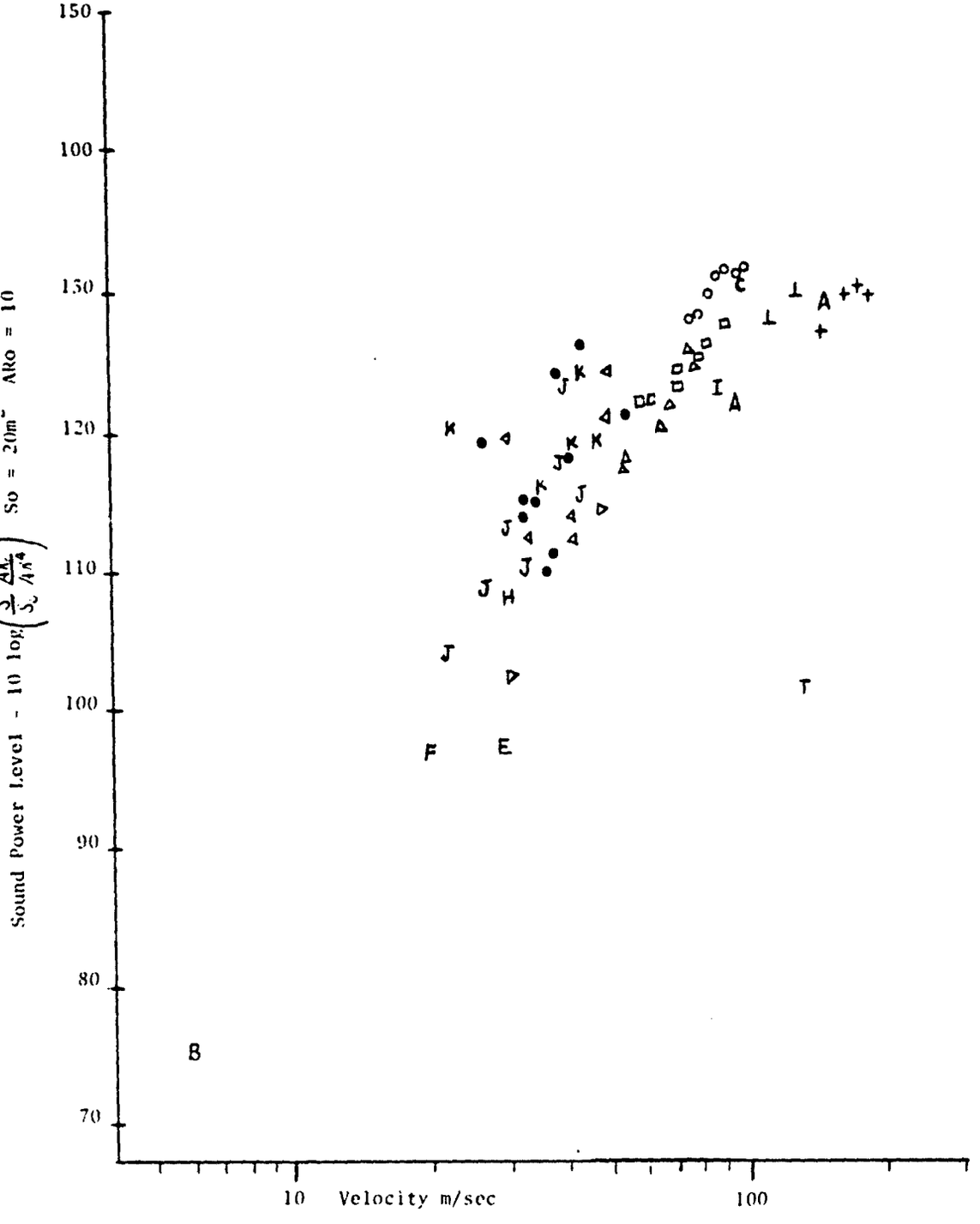

FIGURE 27 Acoustic Power Levels Normalized with S/AR^4

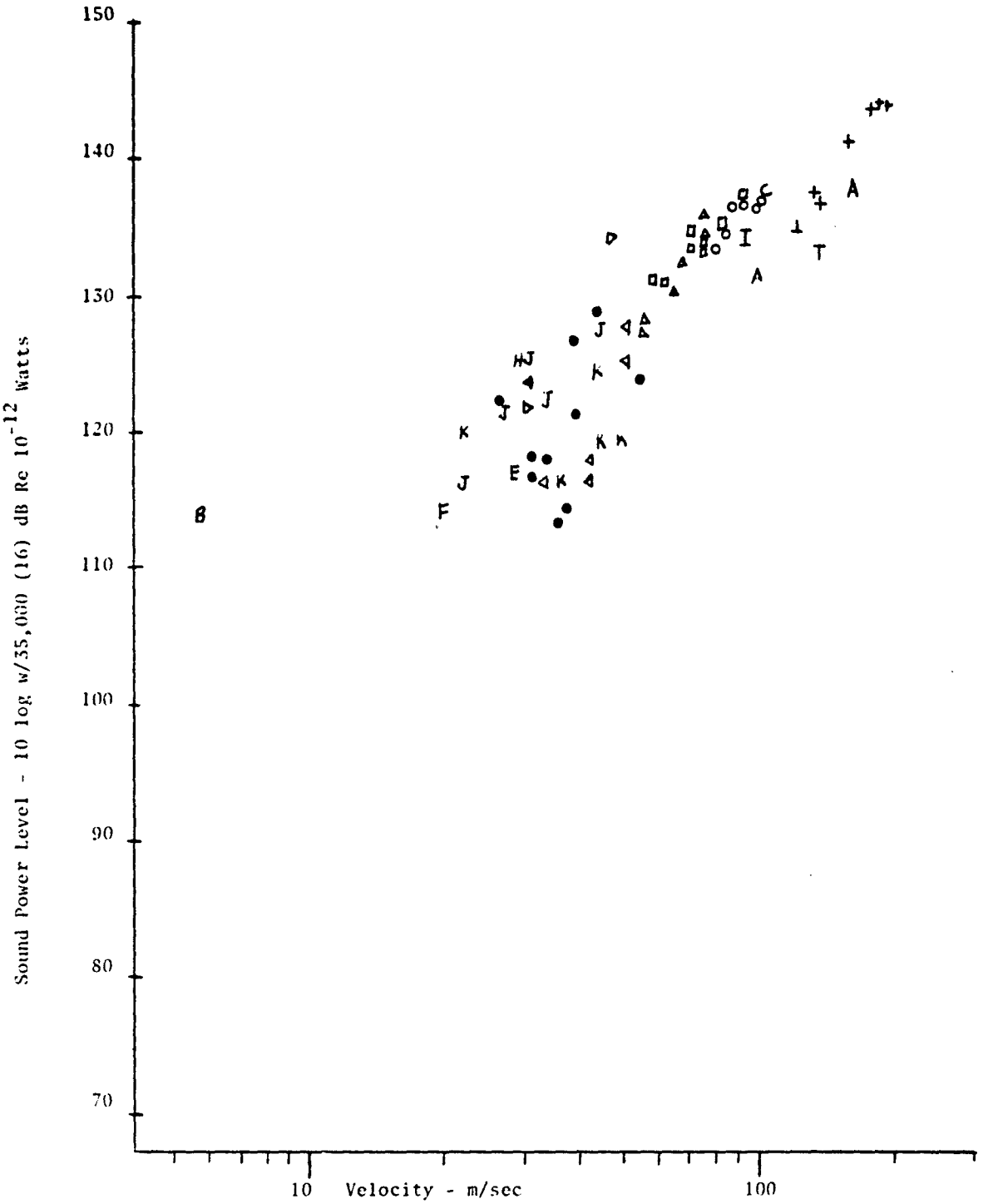

Figure 28 Acoustic Power Levels Normalized with W

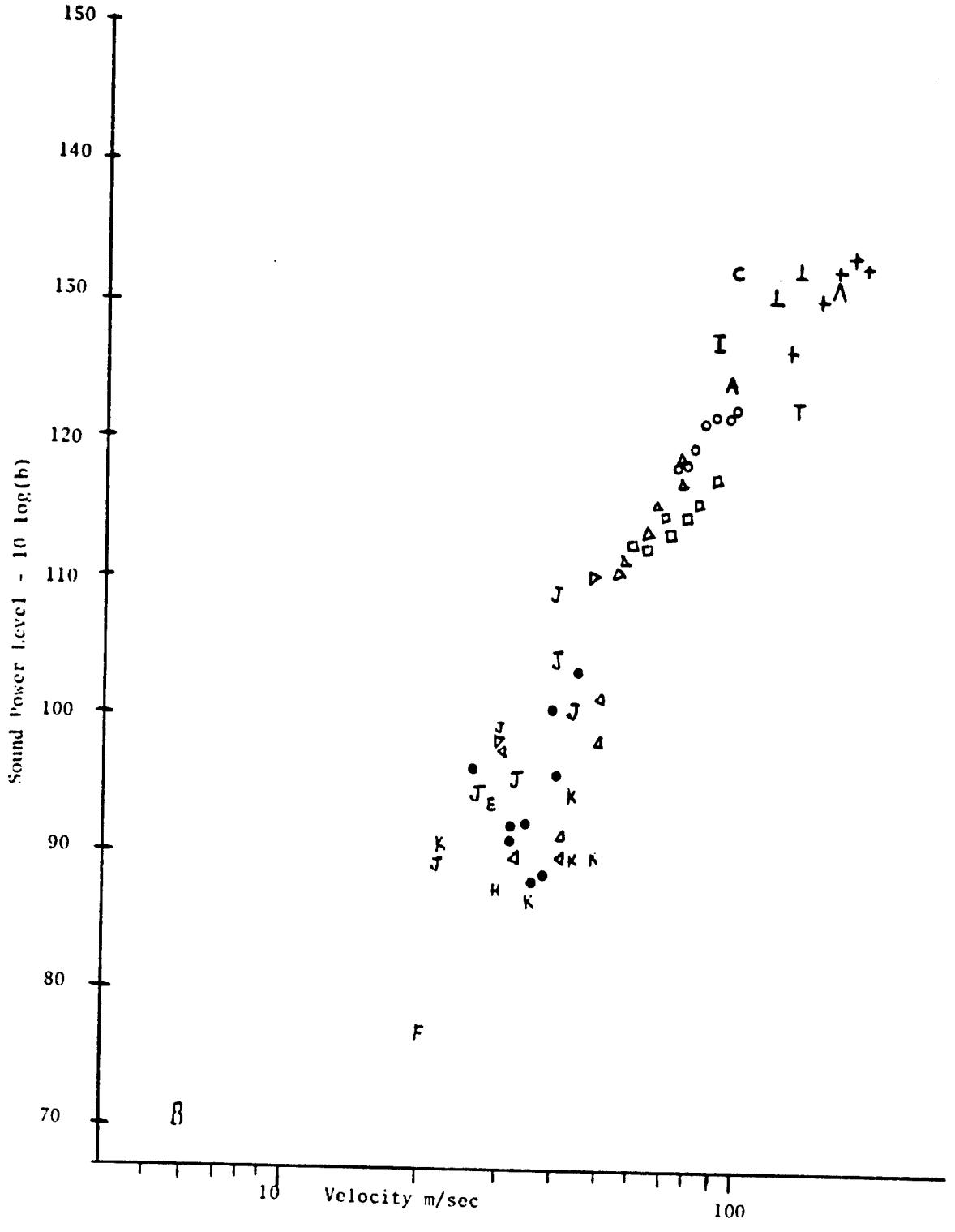

Figure 29 Acoustic Power Levels Normalized with wingspan

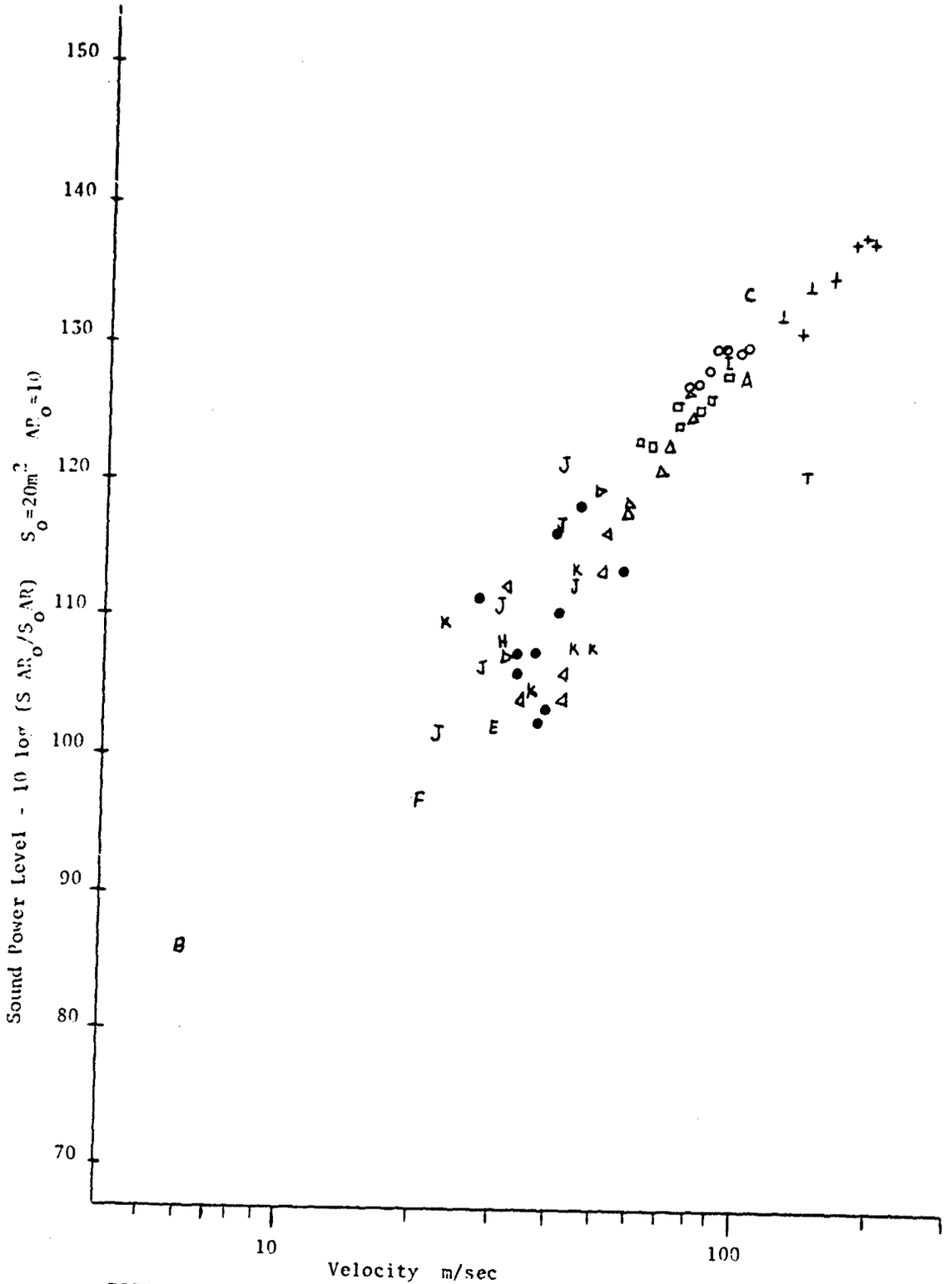

FIGURE 30 Acoustic Power Levels Normalized with S/AR

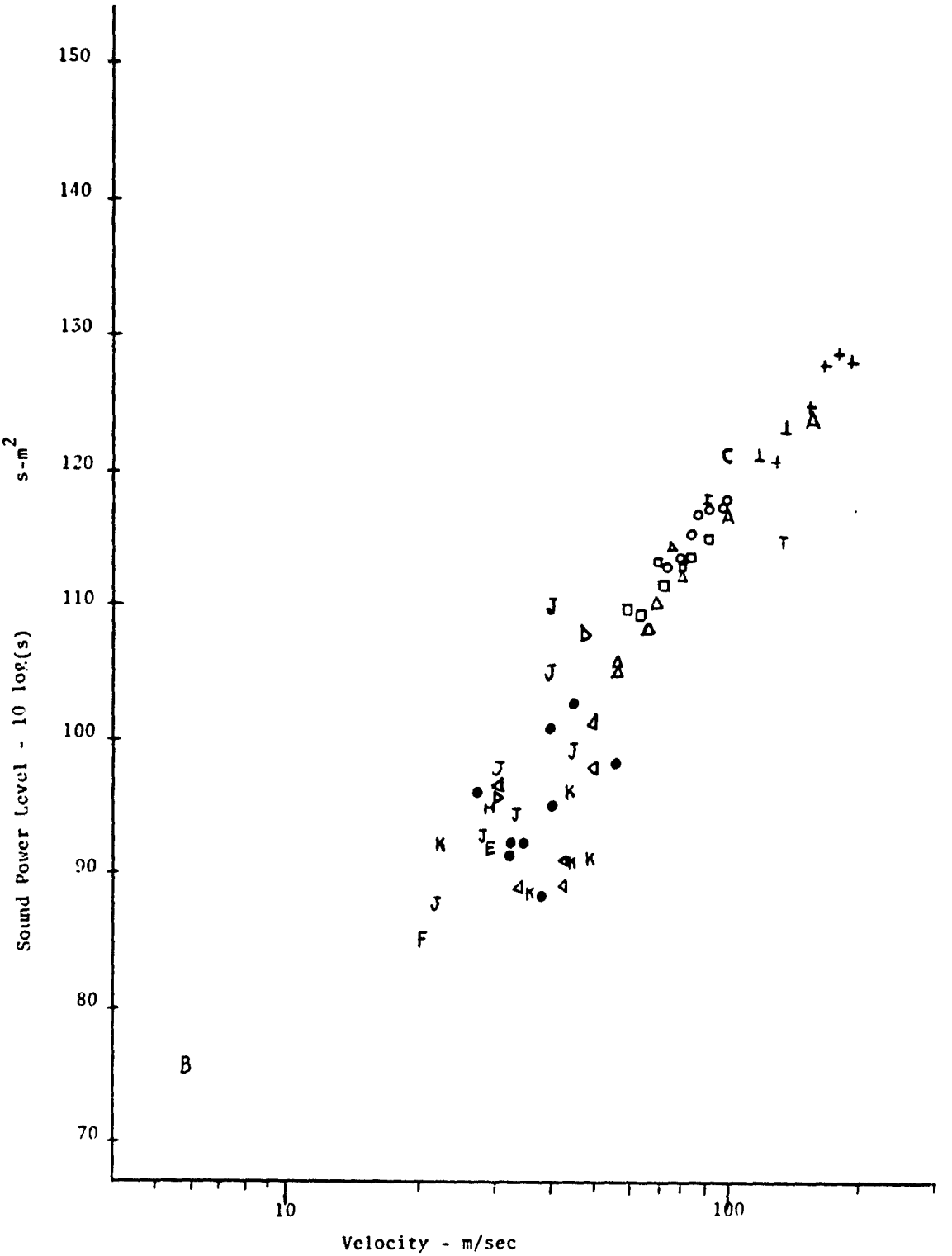

FIGURE 31 Acoustic Power Level Normalized with S

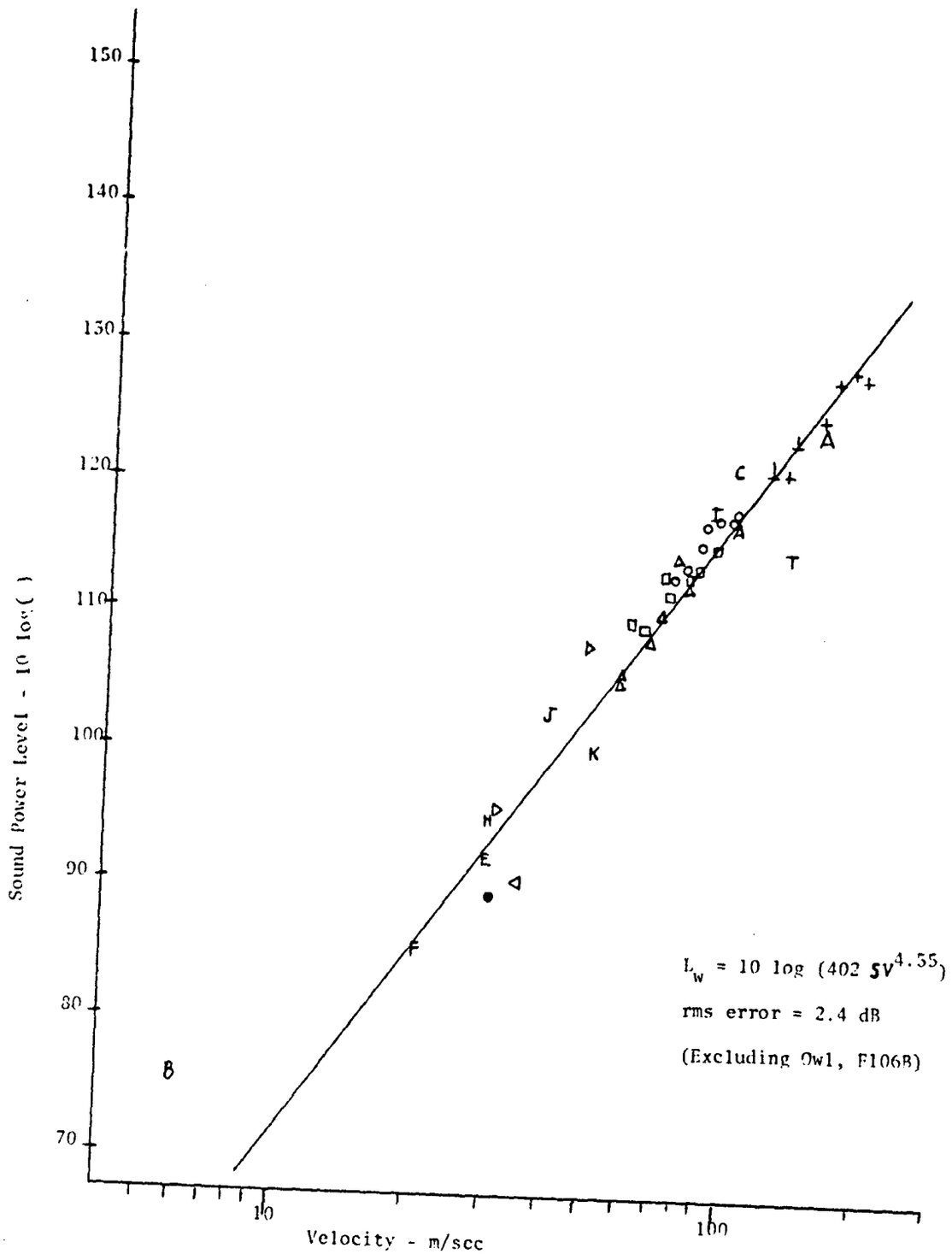

FIGURE 32 Acoustic Power Levels Normalized with Wing Area (S)

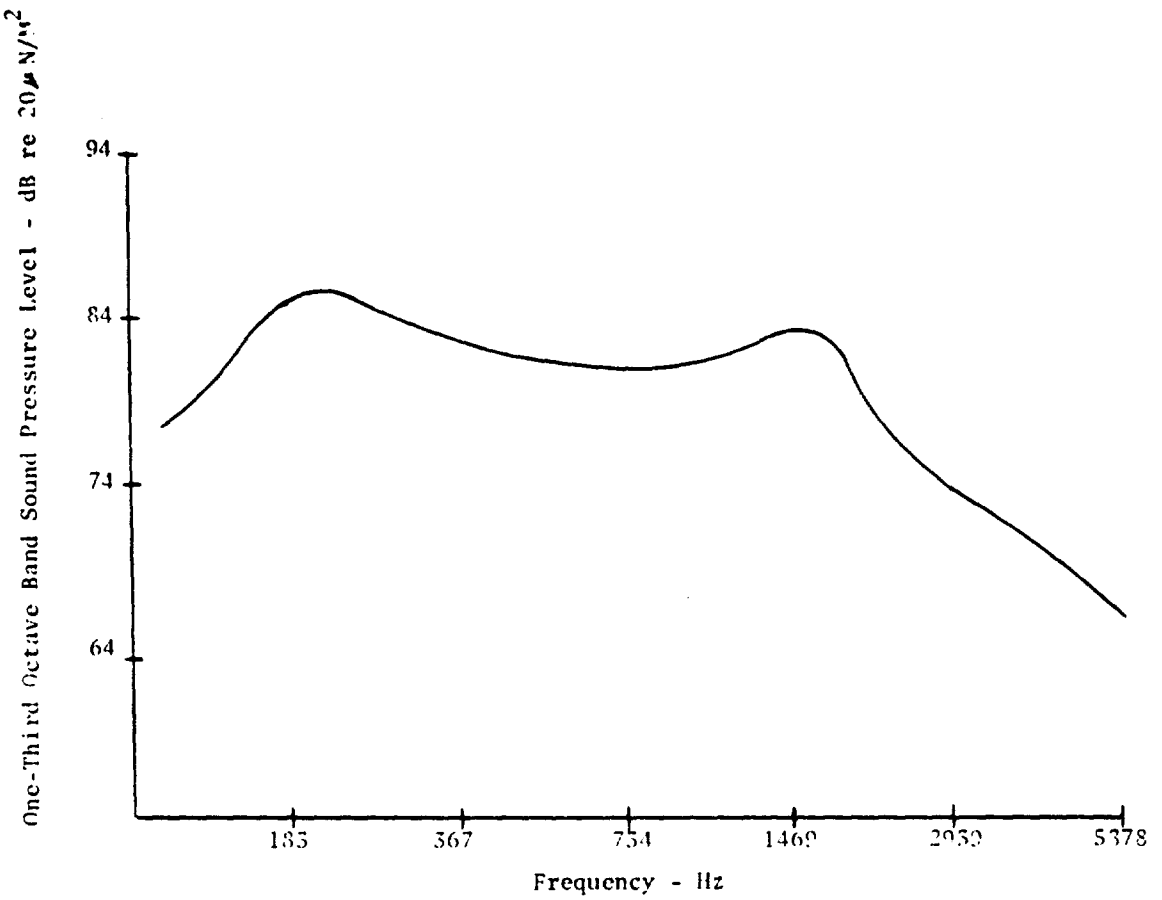

Figure 33 Predicted Flyover Noise Spectrum of a Clean Configured B-747 for an Altitude of 150 m and Velocity of 130 m/s

*U.S.Government Printing Office: 1978 — 657-002/287